2017-01-01

Design Of A 1 Megawatt Heat Input Direct Power Extraction System For Advanced Topping Cycles

Brian Matthew Lovich
University of Texas at El Paso, bmlovich@miners.utep.edu

DESIGN OF A 1 MEGAWATT HEAT INPUT DIRECT POWER EXTRACTION SYSTEM FOR ADVANCED TOPPING CYCLES

BRIAN MATTEW LOVICH

Master's Program in Mechanical Engineering

APPROVED:

Norman Don Love Jr, Ph.D., Chair

Ahsan R. Choudhuri, Ph.D.

Tzu-Liang (Bill) Tseng, Ph.D., CMfgE

Charles Ambler, Ph.D.
Dean of the Graduate School

DEDICATION

This is for my family as well as my friends who have supported me throughout my college education. I could not have done it without their support. This is also possible because of the education I receive from UTEP as well as the guidance of my advisor, Dr.Love. I also would like to acknowledge my coworkers at the cSETR who helped throughout my college career.

DESIGN OF A 1 MEGA WATT HEAT INPUT DIRECT POWER EXTRACTION SYSTEM FOR ADVANCED TOPPING CYCLES

BY

BRIAN MATTEW LOVICH,

THESIS

Presented to the Faculty of the Graduate School of

The University of Texas at El Paso

in Partial Fulfillment

of the Requirements

for the Degree of

Master of Science

Mechanical Engineering Department

THE UNIVERSITY OF TEXAS AT EL PASO

May 2016

ACKNOWLEDGEMENTS

The research is supported by the US Department of Energy, under award DE-FE-0024062 (Project Manager Jason Hissam). However, any opinions, findings, conclusions, or recommendations expressed herein are those of the authors and do not necessarily reflect the views of the Department of Energy.

ABSTRACT

Power development has become a standard for living; as such more efficient and cleaner methods are desired. One such method is that of the direct power extraction system utilizing Magnetohydrodynamic properties. This paper will discuss the combustor designed and developed for a direct power extraction system at the 1 MW heat input range. A short history of the power systems utilized with a focus on the direct power class will be conducted in the first chapter to give insight into the benefits of using the direct power system. Then a literature review the fundamentals of direct power systems will be conducted to give insight into key parameters and background for design methodology. The proof of concept 60 kW combustor of which the 1 MW combustor is based will be reviewed for key parameters. The key parameters allowed for proven methods to be kept constant to match performance; other parameters were derived through a scaling parameter study for proper scaling of the combustor. Next will be an in-depth analysis of the component design methodology of each major section of the combustor, namely the combustion chamber, injector, nozzle, and cooling channels. The driving parameters of each, as well as equations used, will be discussed. To correctly account for phenomena outside the scope of the analytical approach of chapter 2, two main computational models were developed of the combustor. First was the 3-D non-premixed combustion model to ensure injector performance, exit parameters were met, and optimize combustion chamber geometry. A second model of the combustor wall was developed for a combined thermal steady model and static structural model. This combined model was developed to ensure cooling parameters were met as well as predict combined stress within the wall during testing conditions. Both models were developed within Ansys software package. The relative accuracy presented and as well major performance parameters were discussed to assess the design's validity and ensure safety.

TABLE OF CONTENTS

LIST OF TABLES

LIST OF FIGURES

NOMENCLATURE

Area	A
Magnetic Field Strength	B
Constant	C
Constant pressure specific heat	C_p
Speed of sound	c^*
Diameter	D
Electron Field Density	E
Young's Modulus	E
Friction coefficient	f
Gravity	g
Kinetic energy generation due to buoyancy	G_b
Kinetic energy generation due to velocity	G_v
Species enthalpy	h
Overall heat transfer coefficient	h_g
Higher heating value	HHV
Current Density	J
Diffusion flux species	$\vec{J}$
Mass flux	$\mathcal{J}$
Thermal Conductivity	k
Turbulent kinetic energy	$\mathcal{K}$
Length	L
Mach Number	M
Momentum Flux ratio	MFR
Mass flow rate	$\dot{m}$
Nusselt Number	Nu
Power input rating	P_{total}

Pressure	p
Prandtl number	Pr
Volumetric flow rate	q
Radius	R
Net rate of production of species	$\mathcal{R}$
Reynolds number	Re
Rate of creation by addition	$\mathcal{S}$
Total entropy	S
Thickness	t
Temperature	T
Poisson's Ratio	v
Velocity	V
Mass fraction	Y

Greek Letters

Expansion ratio half angle	α
Ratio of specific heats	γ
Dissipation rate	ϵ
Energy	ε
Electrical Conductivity	K
Exit gas momentum efficiency	λ
Dynamic Viscosity	μ
Density	ρ
Stress	σ
Stress tensor	$\bar{\tau}$

CHAPTER 1: MOTIVATION AND BACKGROUND

INTRODUCTION - MOTIVATION

The development of useful electric energy and the methods employed are of great concern in today's society. The demand for electricity increases and regulations on emission become stricter which lends to a need for more efficient as well as cleaner energy development. [1, 2] This thesis focuses on one possible solution to this problem, direct power extraction, and the design of the combustion chamber for this purpose. First current systems are presented to give insight into newer methods. The interworking and popular techniques utilized for power generation will also be a topic of this chapter.

Methods for power generation common today can be broken down into three main categories namely: thermal power plants, kinetic power plants, and alternative methods. Thermal power plants are classified together due to each drawing their power from an initial source of heat. Thermal power plants conclude the energy development process with the steam turbine, a conversion unit that transfers heat into useful mechanical energy. This process involves the heat source converting the liquid water into steam, by indirect heating via a heat exchanger. This steam is then passed through a turbine, which has many blades attached to it. The steam hits and moves the turbine blades causing them to rotate. The blades are attached to a rotor which generates useful electric energy when it spins inside a generator. Now the source of heat can be vastly different and operate at different temperatures. There are nuclear fission power plants, which heat the water using the breaking down of specific atoms, such as Cesium or Uranium [3]. There are also fossil fuel power plants that rely on the burning of coal or natural gas to heat the water.

The kinetic power plants operate by utilizing an already moving fluid. These methods require less operational input as the flow is already in motion rather than forcing a flow via

thermodynamic means, i.e. thermal power plants. The fluid in motion is typical one of the two varieties, either air or water. Air turbines generate electricity from wind and have recently been increasing in use. Another form of a kinetic power plant is the hydro-electric plant which uses moving water to generate useful energy. Hydro-electric plants are typically located near dams and use the difference in water level to drive the water flow. Both start at the turbine stage, continue to the drive shaft, and then lastly the generator. While these operate using no input created by the users, they can't be controlled to the degree of thermal power plants.

Lastly, we discuss alternative power plants. These are the type of energy generation systems that do not utilize the turbine, drive shaft, and generator set-up. These include photovoltaic cells which directly convert sunlight into useful energy or other forms such as fuel cells. While interesting and innovative, they are beyond the scope of this paper and will not be discussed further.

Thermal power plants are the most widely used type in the United States by a considerable margin. Combustion of fossil fuels generates 82% of the energy being used today [4] . The other 18% is split amongst all the other forms. This is the portion of energy generation that would result in the greatest benefit from improvement and the type this thesis focuses.

Power development shifting to that of cleaner methods has been of increasing concern recently. Such efforts to limit pollution have been made clear by such organizations such as the United Nations Framework Convention on Climate Change or the (UNFCCC). Only recently did the UNFCCC pass the Paris Agreement which set high standards on limiting emissions [2]. In terms of total amount, the most abundant pollutant is carbon dioxide. Though almost all other

pollutants are more destructive per unit mass, carbon dioxide is still the most abundant pollutant by a large margin. This can be seen in the graph below.

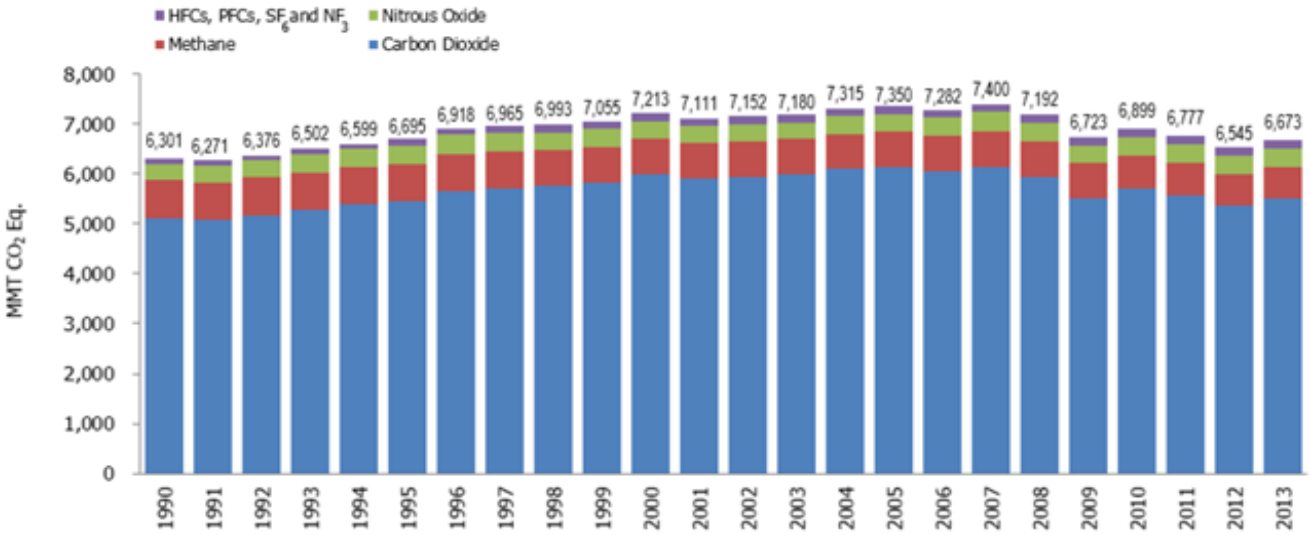

Figure 1 U.S. Greenhouse Gas emissions by gas type [4]

The graph is adjusted for the difference in impact per unit of each pollutant type and is displayed in Millions of Metric Tons (MMT) of CO_2 equivalent. It can be seen that carbon dioxide is and for the most has always been a majority of the emissions representing around 80% at a minimum.

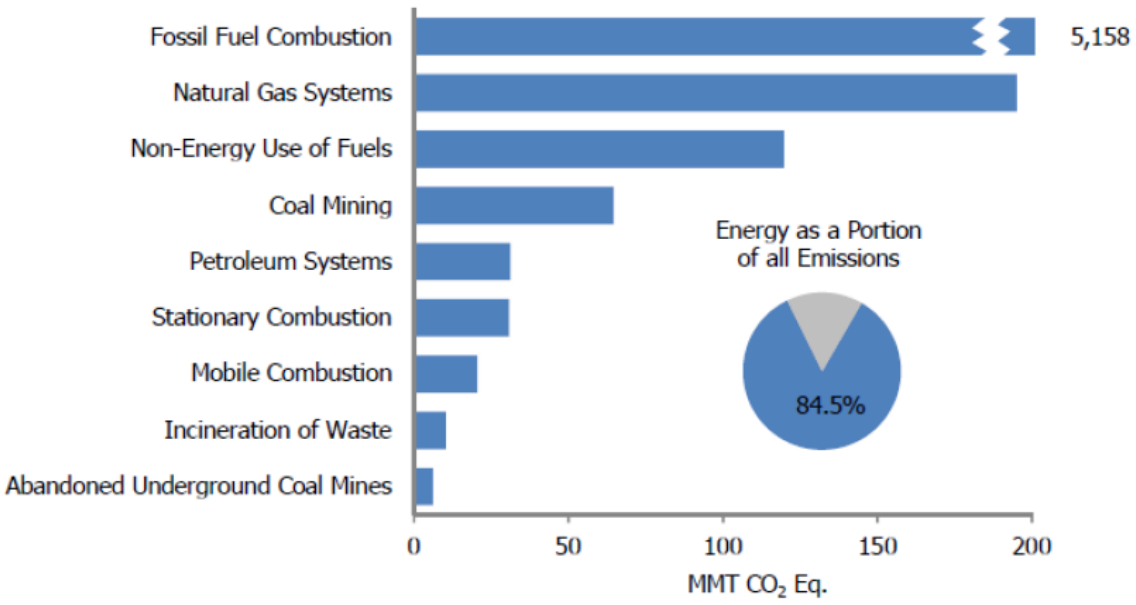

Figure 2 Carbon dioxide contributions by industry [4]

The majority of CO2 emissions are created by energy production. Energy production, more specifically, the fossil fuel combustion variety, accounts for 80% or more of the CO_2 emitted in the US [2] . Restrictions and regulations, such as the Paris Agreement of 2015, affect the production of carbon dioxide specifically, which in turn affects power generation systems that utilize combustion processes.

Greener energy remains a large global concern making greener technology more and more sought after. Methods in development must be competitive in terms of efficiency and meet rigorous regulations put in place by emission standards such as the Paris Agreement of 2015. One such method that can meet such requirements for modern energy development is the oxy-fuel Magnetohydrodynamic (MHD) generator. The MHD generator can both increase efficiency and reduce emissions of the fossil fuel power plants as a topping device.

The MHD generator can allow for the use of oxygen based combustion. The use of pure oxygen as an oxidizer in conjunction with hydrocarbon fossil fuels results in carbon dioxide and water as the products. This would allow for carbon sequestration techniques to be utilized resulting in no harmful emissions being produced. Other forms of combustion result in more complicated products which result in more harmful emissions while also removing the possibility of carbon sequestration. One drawback of utilizing oxygen and hydrocarbon combustion or oxy-fuel combustion is higher flame temperatures of which most steam power plants cannot contain. MHD power generation systems not only contain the higher flame temperatures but requires them. The MHD generator can handle these temperatures as no portions of the system are exposed to the hot gases, in contrast to the turbine blades of the gas turbine. While steam turbine systems can operate at any temperature below a certain threshold, physical limitations of the materials used would require reduction in flame temperature if they utilize oxy-fuel combustion. The higher flame temperatures also results in higher efficiencies as per the 2nd law of thermodynamics. The MHD generator can also be used as a topping system for currently existing steam power plants, meaning the exhaust of the MHD would operate as the heat source of steam power plant as the temperature is reduced after the MHD section [5]. This would increase the overall efficiency of the system to theoretical limits of +70%, while also eliminating carbon dioxide emissions [5].

MHD Literature Review

The Magnetohydrodynamics Generator, or MHD generator, is a type of energy generation system that resembles characteristics of thermal power plant. This system varies from the thermal power plant cycle in that it does not use the steam turbine as a conversion of thermal energy to useful electrical energy; however it does draw power from a heat source. There are two types of MHD generator, open or closed; however this paper is mainly focused the former. The open cycle MHD generation system replaces a solid metal rotor with seeded hot gases as the conductor. This power system starts with a combustion chamber (1) that is connected to a nozzle (2). The combustion products exit the nozzle and then enter a magnetic field (3) and electrode channel section (4). This four step process concludes the MHD portion however modifications can allow this system to be joined with that of a steam power plant as shown in Figure 3.

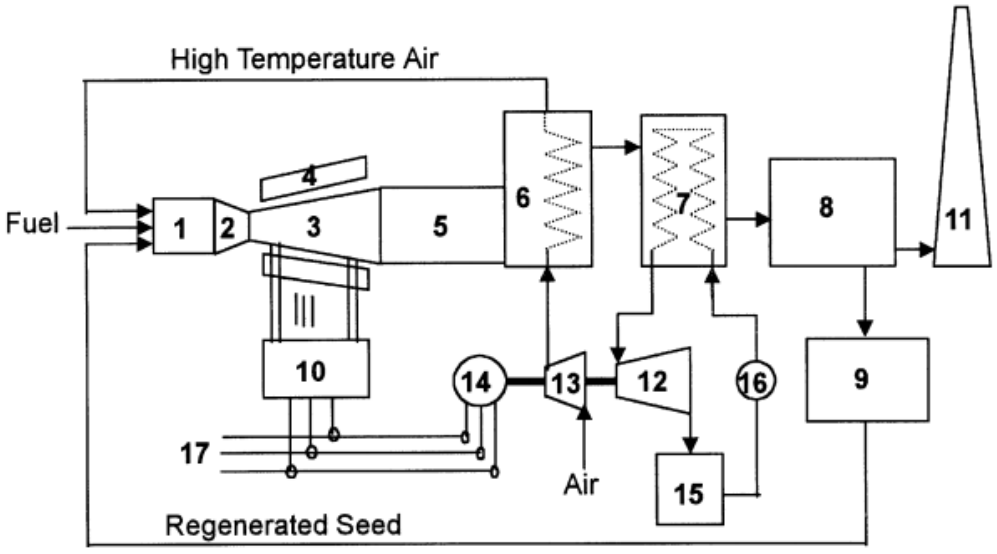

Figure 3 Typical Open cycle gas feed MHD and steam generator cycle [6].

Now we will discuss the main components of the MHD generator and what actions they perform in detail. There is the combustion chamber, which heats up the working fluid: typically

speaking, the nozzle is a De Leval Nozzle, as the electrical output generated is proportional to the speed of the exiting gas. A De Laval Nozzle is one that generates velocities at and above sonic speeds. Most MHD generators operate with gas velocities of Mach 1-4. Now, the gases have to be conductive to act as the conductor, which is achieved by a combination of extreme heat and a seed substance. A seed, when discussing MHD systems, is a substance that can be a strong electrical conductor, in gaseous form, at temperatures of 2300-3000 K [6, 7] . Common seeds are Cesium or the more the popular Potassium and are required to have an electrically conductive gas due to their low ionization potentials [6, 8]. The hot, seeded, supersonic gas is then run through the magnetic field and electrode section. The magnetic field acts to create an electric charge in the perpendicular direction as is dictated by Ohm's general law shown in Eq 1. The electrode section is located to extract the electrical charge from the hot gases to be used to generate useful energy.

$$J = \mathrm{K}(\mathrm{E} + V \times B) \tag{1}$$

The formula shows that if a conductor is passed at some speed relative to the magnetic field, an electric charge is generated. The electrodes are exposed to the exhaust gases and supply a DC voltage proportional to the four variables in Ohm's generalized law. The formula shows that the strength of the magnetic field (B), the conductivity (K), the electron field density (E), and relative speed of the conductor (V) all effect the current density generated (J). Thus, all must be maximized to achieve the highest energy gain. As for the conductivity, it is proportional to T^{10} and thus the highest temperature is considered ideal [5]. The magnetic field is normally generated by a ferromagnetic material, or an electromagnet. The magnetic field is typically on the range of 1-5 Telsa if a strong enough electromagnet is utilized and the speed is normally maxed at Mach 3

depending on the combustion process [9, 10, 11]. There is an inverse relationship between fluid velocity and temperature, as acceleration of the fluid in a nozzle reduces temperature, thus the Mach 2-3 range is considered rather than higher velocities.

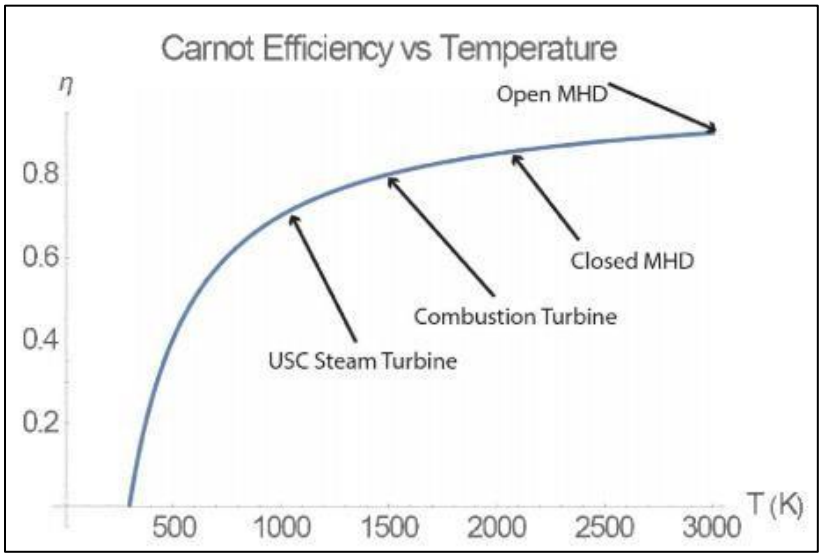

Figure 4 Various Carnot Efficiencies of power generation systems [5].

Open cycle MHD systems typically maximize the temperature due to its large dependence on CONDUCTIVITY of the working fluid. This results in extremely high temperatures, upwards of 3800K in some cases, utilized for the process. Open cycle MHD systems achieve higher Carnot efficiency shown in Figure 4 due to this need for higher conductivity. The higher flame temperatures required of open cycle MHD is how the Carnot efficiency is increased. Oxy-fuel combustion can achieve the higher flame temperatures required for open cycle MHD. Increasing the overall efficiency of a system is one method for reducing emissions, as using less fuel per energy produced will in term reduce emissions per energy produced.

The open cycle MHD power generation system has been as around as early as 1938 [12] MHD systems, which saw considerable use in the 1960's, never fully gain popular utilization due to certain limitations of critical technologies. One of the limitations for the development of MHD systems was the strength of the magnetic field, which is required for the power extraction process. The discovery of niobium-titanium alloys for superconducting magnets' winding led to higher Tesla magnetic fields, tripling the previous maximums. [13]. Other previous limitations included computational power, and higher temperature resistant materials both of which advanced significantly in recent years. The advancements in these limiting technologies has allowed for the open cycle MHD system to have a promising return. [12] The combustor discussed later in the thesis, is to be used for MHD direct power extraction. However many of the intricacies of other components used in this system will not be discussed.

Heritage Power Plants

Table 1 Previous MHD combustor operating conditions [10, 14]

MHD systems	Thermal input (MW)	Fuel type	Temperatrure (K)	Total Mass flow rate (kg/s)
U-02	4.0-9.0	Gas	2900	1.5
K-1	10.0-17.5	Gas	2800	1.5-2.5
BCURA	5.6-8.4	Oil	2800	2.5-2.8
AVCO	12	Oil	3000	2.7
U-25	320	Gas	2500	50
LORHO	20	Toluene	2450	60
ENIN	8.0-9.0	Coal	2570	3.0
PERC	0.77	Coal	2600	0.213

Performance Requirements

The energy industry is undergoing recent changes focusing on cleaner methods. Modern energy generation techniques must be efficient, as well as cleaner in terms of greenhouse gas emissions. One such method, as mentioned in chapter one is the, Magnetohydrodynamic direct power extraction system. This method, though studied previously since 1938, has seen a revival in founding for the capabilities discussed [12]. One such capabilities is to utilize oxygen based combustion. Oxy-fuel combustion is a viable method for improving magnetohydrodynamic power extraction in power plants due to its high flame temperatures. The use of pure oxygen allows for the system to implement carbon dioxide sequestration techniques. This would help existing systems, utilizing MHD direct power extraction as initial heat sources, to be not only eliminate carbon dioxide emissions but to also increase efficiency. The system requires supersonic velocities and extreme temperatures to achieve its efficiency increase. This thesis will discuss specifically the delivery system of such input parameters for use within a direct power extraction system.

The design of such a device that can provide supersonic velocities at extremely high temperatures is similar to that of a rocket engine. Rocket engines, typically used for the thrust they provide, can operate at supersonic velocities up to Mach 4.5 [15]. The exit temperatures of the combustion products can reach up to 3800 K [15].

Ref [14] suggests additional research to understand larger mass flux and thermal (firing) inputs in MHD systems. In this current work, the design criteria of this larger-scale device was determined based on a survey in the literature.

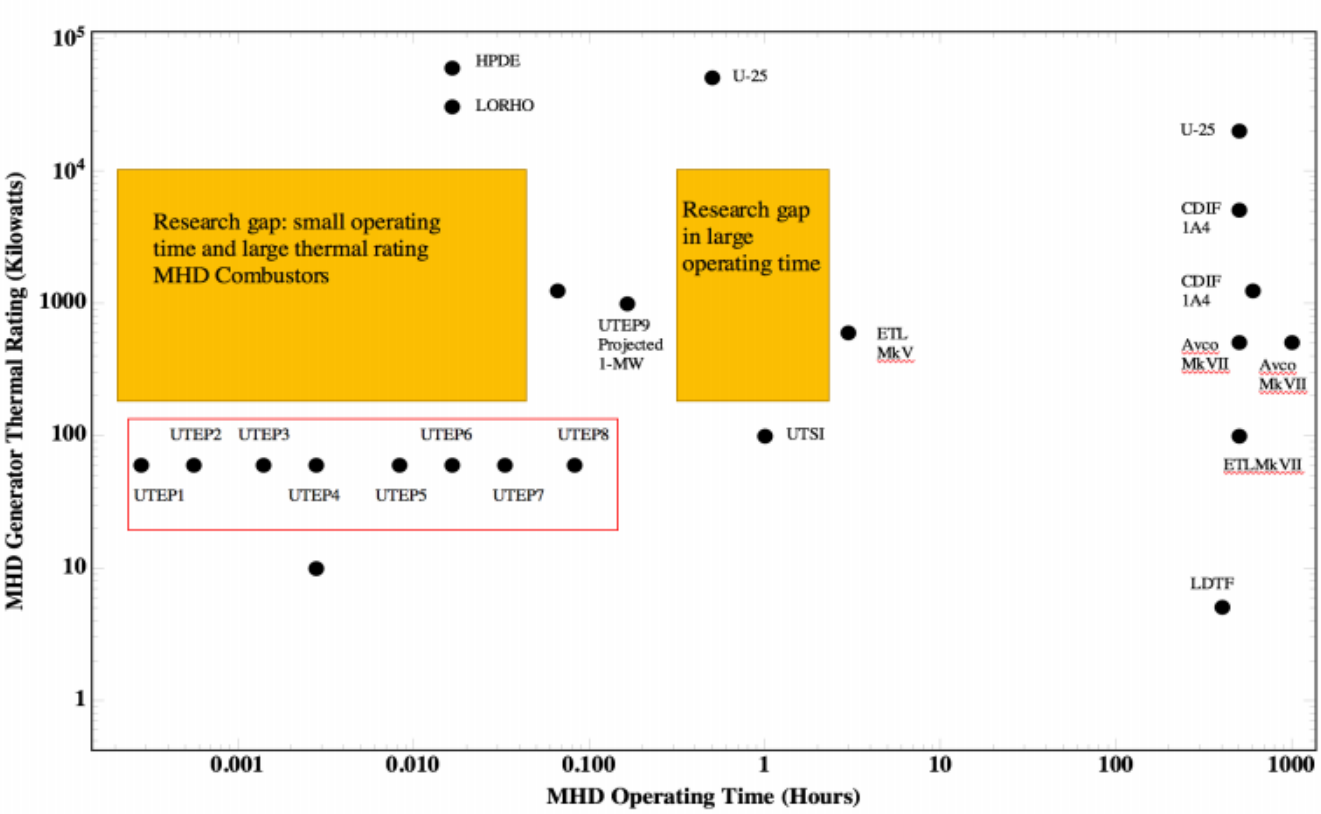

Figure 5 Previous MHD systems (Thermal rating vs. Operating Time)

A gap, associated with this thermal scale, is noticeable in the Figure 5. This then led to the chosen thermal input rating of 1 MW system is unique in that it utilizes pure oxygen and methane compared to the previously used fuel and oxidizer combinations for MHD systems, such as JP4 with oxygen enriched air [6, 14, 16]. The development of multiple power ratings will help lead to non-dimensional scaling parameters specifically suited for modern MHD systems. The characterization of these parameters may lead to much cheaper, much quicker iterations of direct power extraction systems which could lead to rapid acceleration of the technology [17]. Due

to MHD direct power extraction system being intended for extended use, the system for the combustion chamber and nozzle design requires a steady state capability. The exit temperature and exit velocity of the hot gases were decided upon based on design requirements: these values were chosen to optimize the power output of the MHD generator for our given parameter choices and resulted in 2800 K and Mach 2, respectively.

CHAPTER 2: COMPONENT DESIGN & METHODOLOGY

PROOF OF CONCEPT (60 KW) LAB-SCALE COMBUSTOR

The first iteration of an oxy-fuel Direct Power Extraction (DPE) system was started in 2014 at UTEP. UTEP developed and has completed testing of the oxy-fuel combustor, with an initial power rating of ~60 kW [18, 19]. This DPE system was the proof of concept, or lab- scale design, and provided more than 50 successful hot-fire tests. The reliability of this system led to the 1 MW design continuation and provided the foundation for much of the methodology required for the increase power rating system. The first combustor was 18 times smaller in terms of heat input. However, many of the processes used for the initial design are still viable for the development of the 1MW combustor. The 1MW design kept many scaling parameters constant to allow scaling data to be obtained from a comparison. The scaling parameters were determined from literature, such as the MFR ratio, the characteristic length, the convergence ratio, and divergence ratio [17, 20]. Other parameters were required to be kept consistent for other considerations, such as the equivalence ratio to maximize temperature. All critical parameters are listed in the Table 1.

Table 2 Proof of concept design parameters

Design Criteria	
Power rating	60 kW
Equivalence ratio	1.1
Combustor material	Inconel 718
Injector	
Tangential ports	4
Momentum Flux ratio	16
Fuel Pressure drop	20 psi
Combustion Chamber	
Characteristic length	620 mm
Chamber wall thickness	1 mm
Nozzle	
Contraction ratio	8
Expansion ratio	2
Diverging angle	2º
Converging angle	15º

The design of the 60 kW combustor was centered on achieving the exit conditions required at the given heat input. The 60 kW design required gaseous methane and oxygen at near stoichiometric mixtures. It utilized a coaxial swirl injector, with 4 tangential ports to achieve mixing characteristics desired. The four inlet ports combined with the oxidizer inlet led to a momentum flux ratio of near 16 when operating at the chamber pressure of 110 psi.

The main body, broken up into 3 main sections, as well as any portion directly connected to the main body was manufactured out of Inconel 718. The combustor required constant water cooling to operate at steady state conditions. The combustion chamber incorporated 6 cooling channels running axially throughout the combustor exterior to achieve the required cooling for combustor to safely operate. The combustion chamber required a spark ignition port to allow controlled ignition. To assess combustor characteristics and ensure safe operating conditions a static pressure sensor, and a wall thermocouple conduit were included in the chamber wall. Due to the complexity of the cooling channel geometry, which lined the combustor wall from the injector to the diverging nozzle, the combustor was segmented into the 3 sections and laser welded after manufacturing. The combustor chamber, which due to experiencing extreme temperatures near 3300 K, was required to be made of a singular solid body. This action of making the inner wall of the combustion chamber of one part was to eliminate wields that can

weaken the structural integrity. The other two sections sealed the cooling channels with two sections referred to as the cooling jacket. The 3 main sections can be seen below in Figure 6.

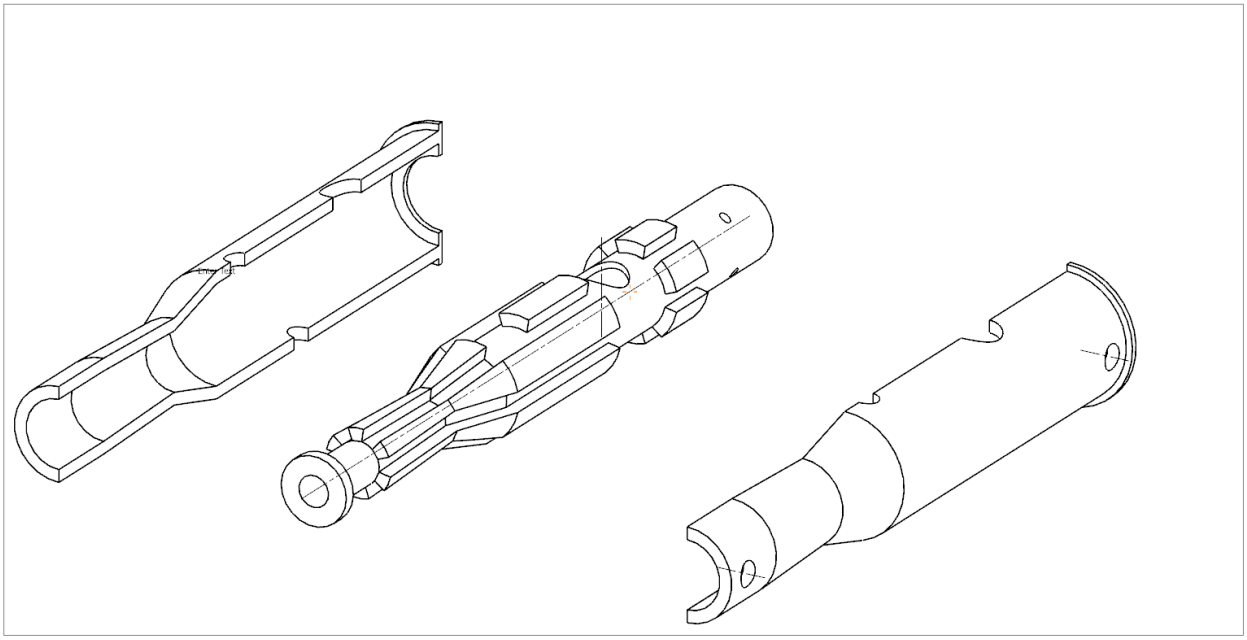

Figure 6 Proof of concept main combustor with cooling jacket exploded view

The design methodology led to extended tests, well throughout the needed longevity of the combustor. The tests gave valuable data into the performance of the 60kW concept design specifically in allowing a comparison to the expected performance of the design methodology. Specifically, the thermocouples placed in the water before and after cooling the combustor as well as the thermocouple located at the combustor wall between the igniter and converging section. Comparing the change in water temperature to predicted values allowed for an analysis of the design methodology accuracy. The water heated up by 2.1 K as compared to the predicted value of 3.2 K [21]. This is to be expected as the cooling system was oversized in terms of cooling capacity to prevent undercooling and possible thermal failure from occurring. The temperature of the combustor wall at the specified location was within 10 K of the predicted value, again below

the predicted value [21]. This can also be attributed to the higher cooling system capacity and results in an error of less than 10 %. This results in a proven accuracy of the change in water being near 1 K of the expected value, the accuracy of the wall temperature within 10% error, as well as the 100% success rate for the hot fire tests of the proof of concept design. Due to the 60 kW concept design showing promising results, the 1 MW system utilized a very similar design methodology.

ANALYTICAL APPROACH

The heat input rating was the starting point of the design and was determined by the fuel flow rate required to provide the 1 MW power rating. This was found using the higher heating value of methane, the chosen fuel, and then determining the amount of methane needed to supply the power rating. Due to thermal stress, approximations in the combustion chamber section, the higher heating value was considered for a worst-case scenario approach.

$$\dot{m} * HHV = P_{total} \tag{2}$$

In this equation $\dot{m}$ is the mass flow rate of methane alone, HHV is the higher heating value for the fuel and P_{total} is the power input. The HHV of methane is 55.5 MJ/kg [22]. Using this data, the mass flow rate of a system was found to be 18 g/s.

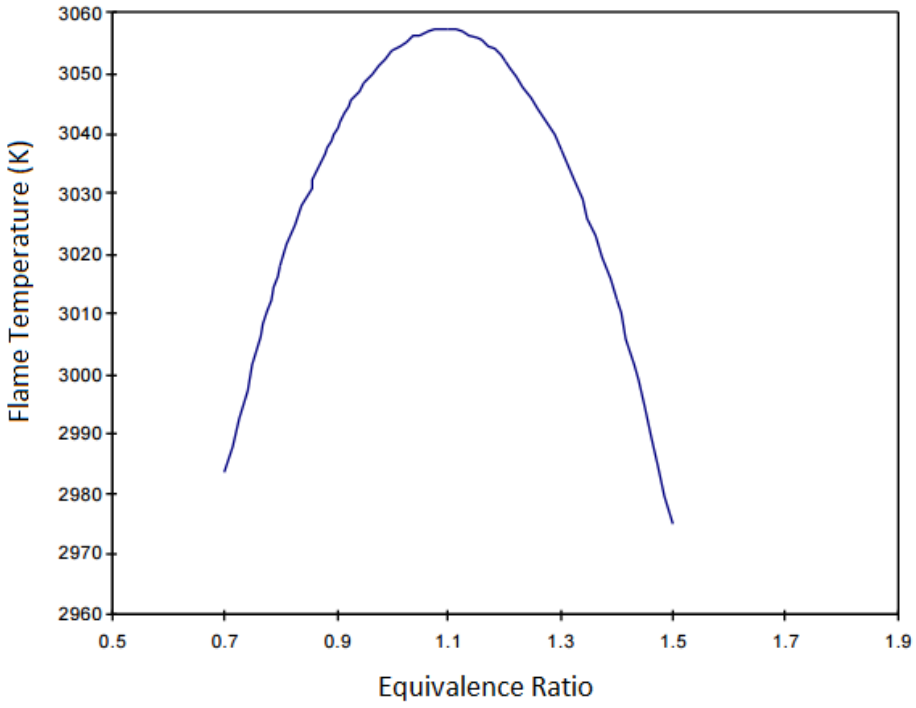

Figure 7 Equivalence ratio of methane and oxygen vs flame temperature [23].

The equivalence ratio was selected to achieve the highest adiabatic flame temperature for pure oxygen and methane [23]. MHD systems rely heavily on the conductivity of the fluid, which is proportional to the temperature: the highest possible exit temperature of the combustion products is desired for more efficient power generation, as known with the second law of thermodynamics (Carnot efficiency). As it can be seen from Figure 7 for methane and oxygen combustion, an equivalence of around 1.1 results in the highest flame temperature. The values for the flame temperature at our operating pressures will be found using various computational methods as well as empirical methods to be compared with literature.

This value for mass flow of methane combined with the mass flow of the oxygen, calculated from the equivalence ratio, was used to determine the minimum throat diameter. This was found with the properties of the throat for supersonic nozzles. The flow will be choked at the

throat which combined with the given mass flow, results in knowing the minimum area the throat can be. This was found to be 15.89 mm for the mass flow required for the 1 MW heat input requirement.

Combustion Chamber

The combustion chamber uses a thin walled, counter flow cooling channel design. The design centered around accounting for thermal stress and scaling parameters determined to focus on combustion stability [17]. The design methodology was similar to that of liquid propellant rocket engines, with modifications to enhance combustor efficiency and thermal to kinetic energy conversion. The design and assumptions used in the methodology will be discussed in this section.

For any calculation to begin for our combustor, the properties of the fluids used had to be determined. These can be found using an analytical approach with a strong background in combustion, fluid mechanics, and compressible flow. One other method for finding many of the parameters needed, which was checked with the analytical approach, was utilization of NASA's CEA code. [24] NASA CEA or Chemical Equilibrium with Applications solves compressible flow equations for rocket engines when considering full combustion upstream. NASA CEA requires many inputs to be known beforehand, such as chamber pressure and equivalence ratio, however is very reliable for the combustion process used in this design. The 60-kW design utilized NASA CEA and the 1 MW design methodology also incorporated its use. Its main function was for finding the required parameters for other calculations such as thermal stress.

From this, assuming full combustion, the constant pressure specific heats, ratio of specific heats, and the Prandtl number at the chamber, throat and exit properties could be found.

These were then used to find the overall heat transfer from the combustion gases to the wall, as well as other calculations, to help in the design of the wall for the combustion chamber.

An important parameter for the design of a combustion chamber was the thickness of the wall. Wall thickness, alongside the chamber pressures required, determines safety factors for chamber material. To correctly determine the factor of safety of a combustion chamber, it is of vital concern for safety and combustor longevity. This parameter was found using the equation for combined stress presented in Eq. 3 [15]. One parameter required for the thermal portion of the combined stress equation is heat flux to the chamber wall. Bartz's equation was used to find the heat transfer coefficient for the gas side from the combustor [15]. The Bartz's equation is often employed to determine the heat flux at any point axially in rocket propulsion design. The heat flux at the throat is known to be the highest in magnitude and was thus the main concern for thermal stress.

$$h_g = \left[\frac{0.026}{D_t^{0.2}}\left(\frac{\mu^{0.2}C_p}{Pr^{0.6}}\right)\left(\frac{(p_c)g}{c^*}\right)^{0.8}\left(\frac{D_t}{R}\right)^{0.1}\right] \times \left(\frac{A_t}{A}\right)^{0.9}\sigma \tag{3}$$

Where the parameter σ is presented in Eq. (4):

$$\sigma = \frac{1}{\left[\frac{1}{2}\frac{T_{wg}}{(T_c)_{ns}}\left(1+\frac{\gamma-1}{2}M^2+\frac{1}{2}\right)\right]^{0.68}\left[1+\frac{\gamma-1}{2}M^2\right]^{0.12}} \tag{4}$$

Using this approximation, along with cooling parameter assumptions such as coolant side wall temperature, the heat flux was determined to be 8.77 MW/m^2. The heat flux

determined is similar in magnitude to the proof of concept design experimentally measured heat flux of 7.76 MW/m^2.

Knowing the heat flux the enables the combined stress to be utilized. The only unknowns left in the combined stress equation are that of thickness and the total stress.

$$S_t = \frac{(p_{co} - p_g)r}{t} + \frac{Eaqt}{2(1-v)k} \tag{5}$$

An iterative method was employed to determine the design space of which the combustion wall can operate. The wall thickness was initially assumed and varied from 0.5 mm to 10 mm in increments of 0.5 mm. Each case was then plotted and compared to the yield strength of the combustion chamber material at the temperature known from the Bartz's equation assumptions.

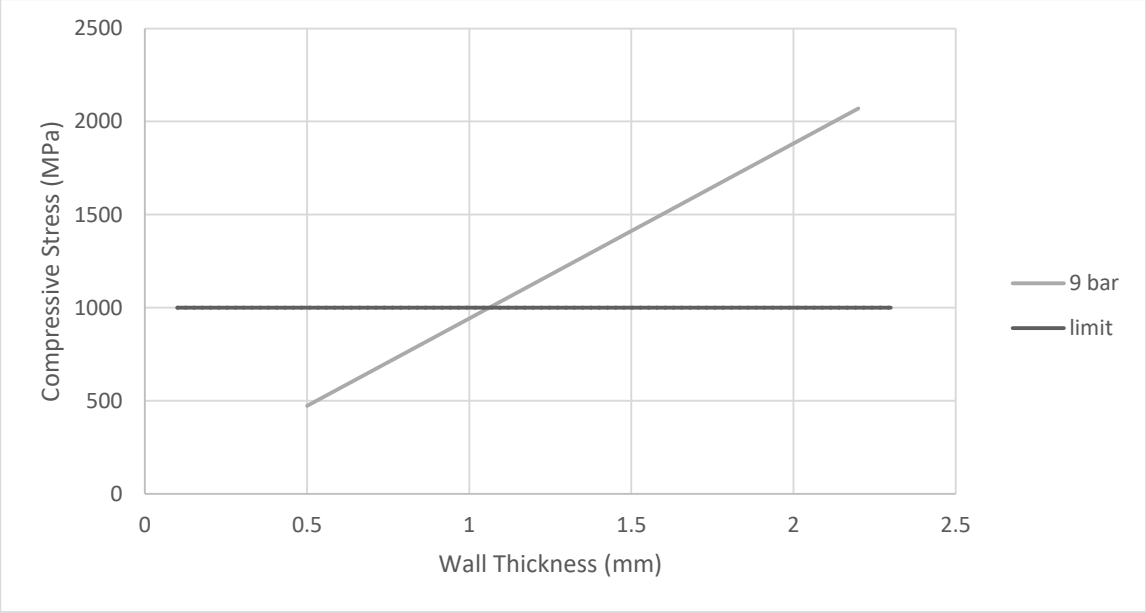

Figure 8 Total stress as compared to combustor wall thickness.

The combined stress increases as the thickness increases. Under the consideration of purely mechanical stress, increasing the thickness would decrease stress as shown in the mechanical part of the stress shown in Equation 6.

$$\sigma_{mech} = \frac{(p_{co} - p_g)r}{t} \tag{6}$$

This mechanical portion results in <10% of the total stress. The thermal stress is represented by the portion in Equation 7.

$$\sigma_{thermal} = \frac{Eaqt}{2(1-v)k} \tag{7}$$

This section of the combined stress is proportional to the thickness. Due to the operating pressure of 9 bar, and the heat flux being 8 MW/m^2, the thermal stress contributes the remaining >90% of the stress. The thermal stress is thus the determining factor and decreasing thickness reduces stress. While theory dictates reducing the wall thickness more, a wall that is too thin will result in fabrication issues and thus must be above a certain physical limitation.

Nozzle Design

The system requires an exit velocity to be achieved for efficient power generation. Over expanding of the nozzle can cause shock waves to propagate within the direct power extraction system which would be detrimental for system longevity. Conventional rocket engine design was considered however many parameters critical for most engine design, such as weight of the engine, are not applicable in the current design process since the system will be used for terrestrial applications.

The nozzle section was critical for correct supersonic exit velocities to be achieved. For a converging diverging nozzle the flow will be Mach 1 at the throat if the pressure ratio is above the critical pressure ratio [15]. The throat diameter is found by assuming supersonic conditions for a given mass flow. This must be ensured for the exit parameters to be supersonic, and one of the required operating conditions is an exit velocity considerably above 1100 m/s. To have a grasp of the shape of a typical nozzle section an image is provided in Fig. 9. P_c represents the pressure at the end of the combustion chamber, Pt is the pressure where the throat is located, and P_e is the pressure at end of the nozzle section.

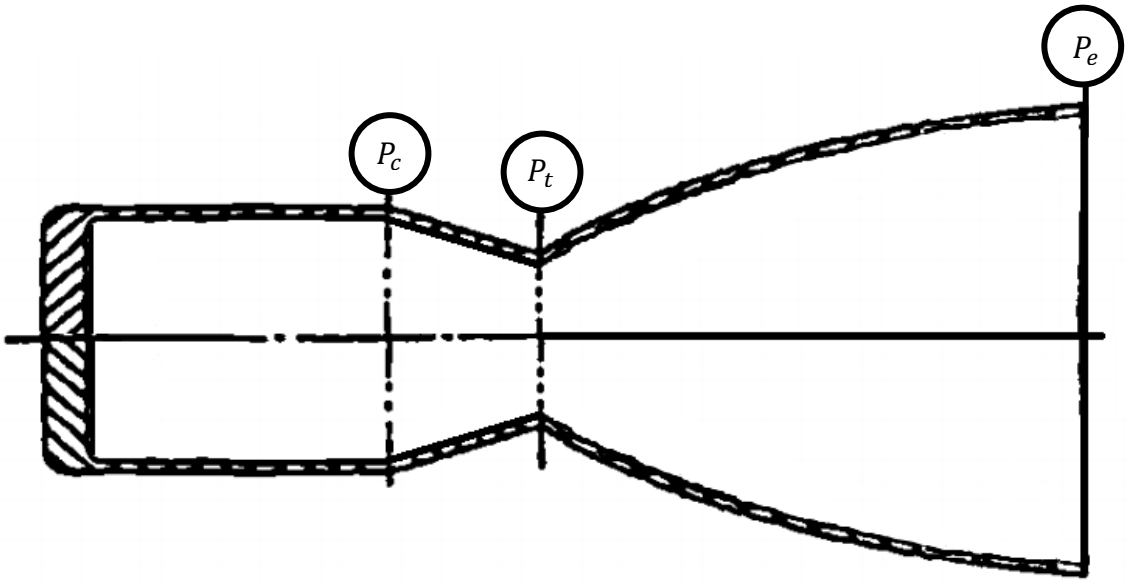

Figure 9 Rocket engine diagram of pressure locations considered for nozzle design [15]

The nozzle is the variation of the combustion chamber radially and the design of which affects the exit conditions. Nozzle design includes many empirical methods of which prove to be useful. The main concern when discussing the nozzle is the effects it will have with combustion

stability and to the heat transfer to the wall. One such parameter was the expansion ratio, which is the rate at which the throat diameter is expanded downstream to the exit diameter. Typically with rocket engines, this is done at as fast a rate as possible to save space in the axial direction, as well as minimize the heat transfer to the wall. This is due to the purpose of the rocket engine, which is mainly providing thrust. Thrust is a function of exit velocity and independent of exit temperature. The main requirement for direct power extraction is to extract as much energy as possible which is directly linked to exit temperature as well as exit velocity. The equation below shows the relationship between the half angle of the expansion ratio and its effect on exit gas momentum [15].

$$\lambda = \frac{1}{2}(1 + \cos(\alpha) \tag{8}$$

In this equation λ is the exit gas momentum efficiency, and α is the half angle for the expansion ratio. When $\alpha = 0$ the exit gas momentum efficiency is theoretically 100%; however, this is impossible as the diverging section of the nozzle would need to be infinitely long. For rocket engines there is a limit to the exit gas momentum efficiency based on the tradeoff of the added material. An increase in mass of the rocket would literally out weight the benefits of the increase in exit gas momentum efficiency. The weight of the direct power extraction system is negligible and thus a much greater momentum efficiency can be used. The half angle decided upon based on these parameters is 2º, which results in an exit momentum efficiency of 99.96%. This efficiency is considerably higher than the 93.30 % typically found for rocket engines with 30º half angles.

One other thing to note for this design is the relatively low expansion ratio. The expansion ratio was found to increase the velocity only to the requirement of our system, which is built to supply this fluid at higher temperatures and relatively low velocities. The exit conditions are an exit temperature of 2800K and an exit velocity of 2000 m/s. The fluid obeys conservation of energy meaning the converging diverging nozzle simply utilizes thermal energy to increase pressure and converts it to kinetic energy. For rocket propulsion, complete conversion of potential energy to kinetic energy is ideal, as thrust is mainly a function of velocity. When only considering thrust, propulsion rocket engines expansion ratios can be 5 or more likely much greater. This is in contrast to the direct power extraction system which is focused on both velocity and temperature. With these considerations expansion ratio of 1.81 was chosen. Since decreasing the half angle for our system doesn't affect the total length of the combustor as much as it would if it had a larger expansion ratio, high exit momentum efficiencies can easily be achieved without affecting the combustor length significantly.

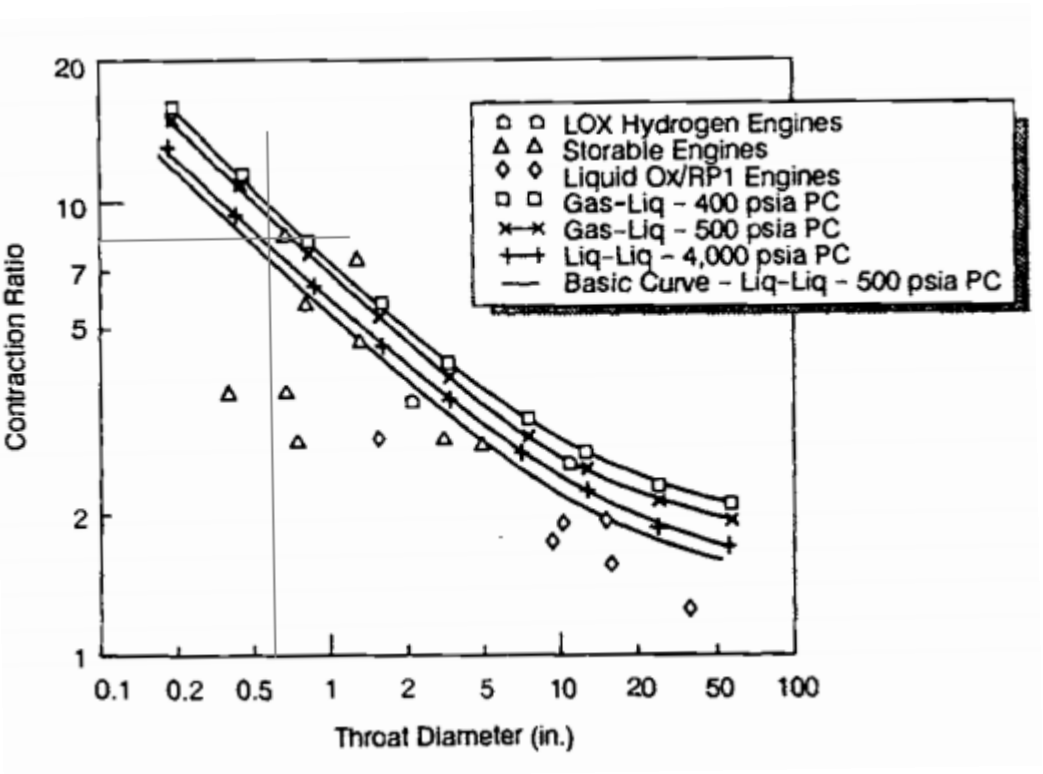

Figure 10 Contraction ratios based on throat diameter [15]

The next subject for discussion is the contraction ratio. A literature review as conducted and a valuable and reliable source was found that specifically discusses the scaling of the contraction ration with respect to the throat diameter. The throat was found to be 16.1 mm discussed in the combustion chamber section, based on requirements, for instance the total flow rates of the fuel and oxidizer. This parameter is shown as the grey lines intersecting in the Figure 10 showing a contraction ratio of 8.

Cooling Parameters

The extreme conditions of the combustion require strong mechanical property material as well as longevity of working life. The extended use of power generation systems' requires extended hot firing. While metallurgical development has been impressive, no material known can withstand the conditions of this type of combustion chamber for long duration without cooling. This led to the utilization of a cooling system for the 1 MW oxy fuel combustor.

To determine the cooling required of our system, the hottest point in the design is to be found and taken into account. Overcooling could lead to lower efficiencies and precautions/design of latter iterations should attempt to mitigate this loss. Undercooling can lead to sudden structural instability, and in turn a catastrophic failure. With this in mind the cooling was designed slightly above that which is determined from calculations. This allows for some error and ensures undercooling is safety avoided.

The heat flux being released to the cooling system varies axially; however, it was designed for the hottest point of the combustion chamber inner side. This was determined in combustion chamber geometry to be at the throat. Knowing that the heat out of the combustion chamber wall must be equivalent to the heat absorbed by the water, the required heat transfer coefficient can be found. The overall heat transfer coefficient is a function of multiple parameters of which have not been set such as hydraulic diameter and coolant flow rate.

The method of implementing cooling channels is anticipated and beyond the scope of this thesis. The design of effective cooling channel geometries to be used in regenerative cooling engine systems and similar designs is a complex and heavily studied topic. Though the cooling

channel design is not required of this thesis, the required flow rates as a function of various hydraulic diameters were developed to ease the selection of the final cooling channel design.

Knowing the heat flux from the previous section of thermal stress analysis allows for the cooling channel requirements to be known. The Sieder-Tate equation was employed to estimate the required flow rate of the coolant fluid for various hydraulic diameters [15]. The properties of the coolant fluid and the material were chosen at the hot side wall temperature of 550ºC and using the heat flux at the throat. The use of the throat heat flux ensures that over cooling is conducted and that wall material properties are above required.

$$Nu = C_1 Re^{0.8} Pr^{0.4} \left(\frac{\mu}{\mu_w}\right)^{0.14} \tag{9}$$

This was plotted in Fig. 11 to show the relationship between volumetric flow and hydraulic diameter, which is linear. The relationship is linear since the velocity is the main parameter that determines the overall heat transfer coefficient.

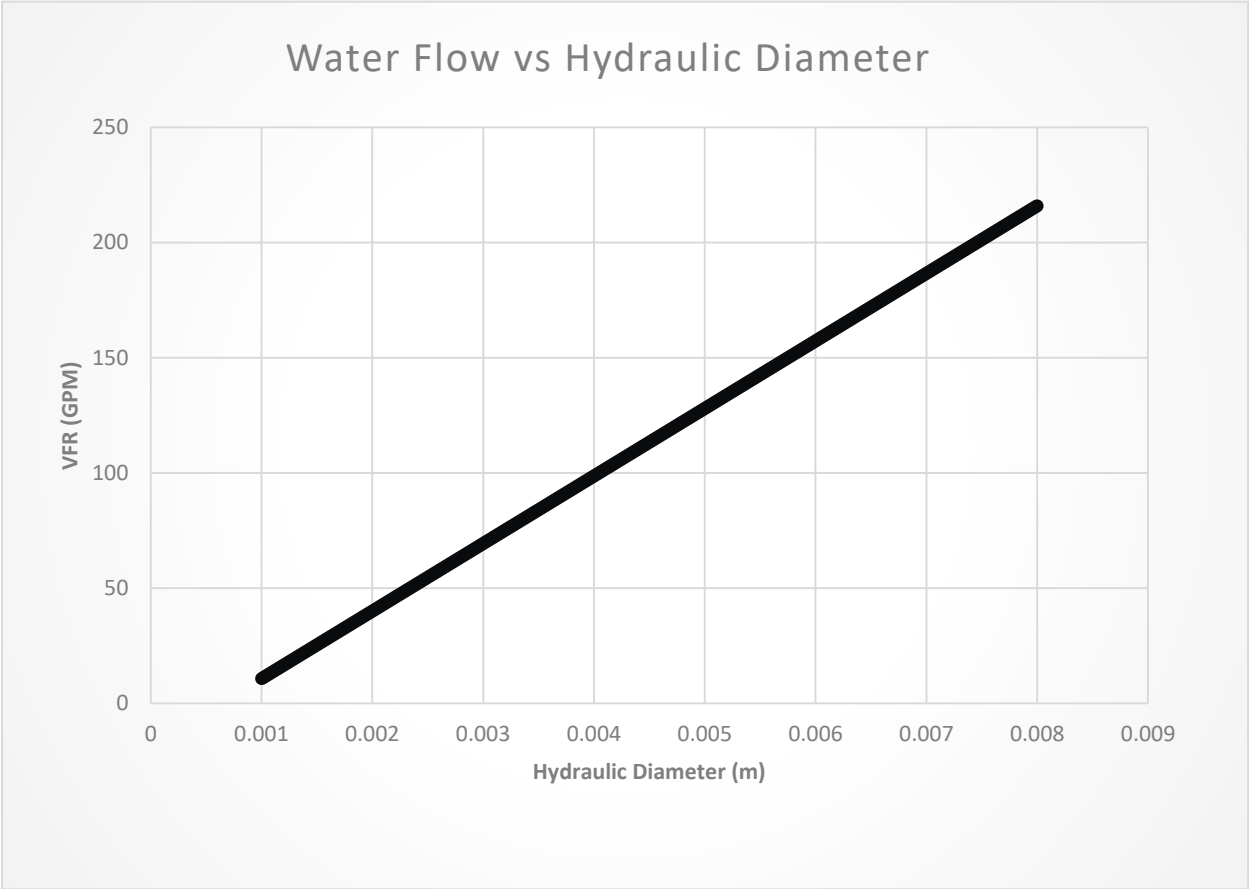

Figure 11 Hydraulic diameter vs Volumetric Flow Rate of the 1 MW cooling channels

The Sieder-Tate equation is specialized for flow through a channel and proved to work very close to intended through validation of both experimental and computational methods. In terms of design a fluid velocity is not directly provided nor measureable. The volumetric flow can be measured and found, and knowing the cross sectional area allows for local velocity to be determined. One other thing to consider is that while a velocity can be found, it does not necessarily mean it can be produced physically. A hydraulic diameter of 20 cm would require 700 gpm, which is considerable in terms of pump power and reservoir size. To also give insight

into what would be an acceptable flow rate the pressure drop through the channels was approximated using internal flow pressure drop equations [25].

$$\Delta p = \left(f\frac{L}{D}\right)\frac{V^2}{2g} \tag{10}$$

A plot was developed to estimate the pressure drop through the channels for different hydraulic diameters, Fig. 12. Using these plots and considering other aspects of the cooling channels, such as machinability and scaling from the initial design allows for this to be developed further.

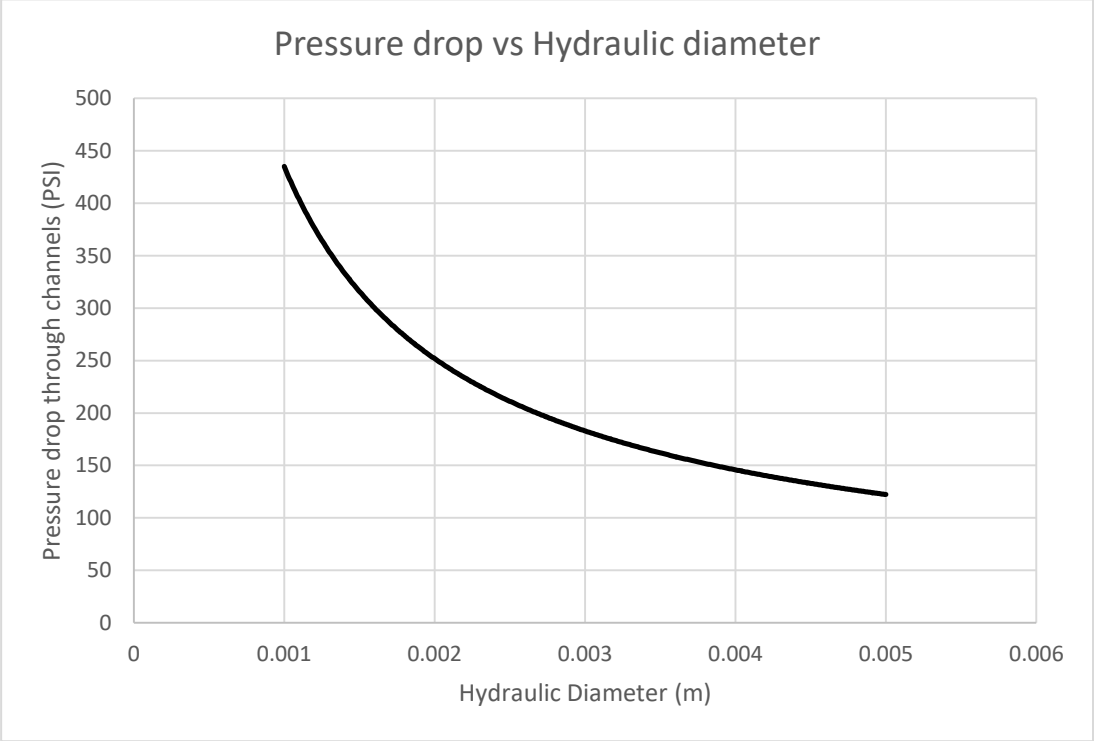

Figure 12 Pressure vs hydraulic diameter for our required flow velocities

Injector

When discussing engines that do not pre-mix the fuel and oxidizer, the injector is critically important. The injector design results in many crucial parameters in terms of direct power extraction safety. The most critical aspect of injector design being the combustion stability of the system. This is due to large oscillations in the combustion chamber pressure and temperature. To isolate the lower frequency oscillations the combustion chamber is constrained by a large pressure drop in the injector. This large pressure drop is normally accomplished by making small orifices, typically on the order of a centimeter to millimeter scale, which induces high velocities to isolate the chamber in terms of fluid velocity as well. The pressure drop dampens the oscillations and helps to ensure upstream conditions of pressure and velocity. Huzel states which values are typically used for what would be considered a high enough pressure drop, being one that is between 15-20% of the chamber pressure [15]. This was design criteria is for liquid propellant rocket injectors however the reasoning to isolate oscillations to the combustion chamber holds true for our combustor and no other source was found for gas-gas engines. The range being 15 to 20% combined with the conservation approach, which this design process is centered, led to the 20% pressure drop requirement [15].

While the design of the injector for the proof of concept design was successful, this design will not work for the larger 1-MW model. This is due to the 18 times increase in flow rates causing much higher pressure drops and velocities if the design was to be unchanged. The design of the 1MW injector must be scaled from the initial proof of concept design, which was a swirl coaxial injector. This swirl coaxial injector has 4 tangential inlet ports that swirl the oxidizer flow to induce mixing.

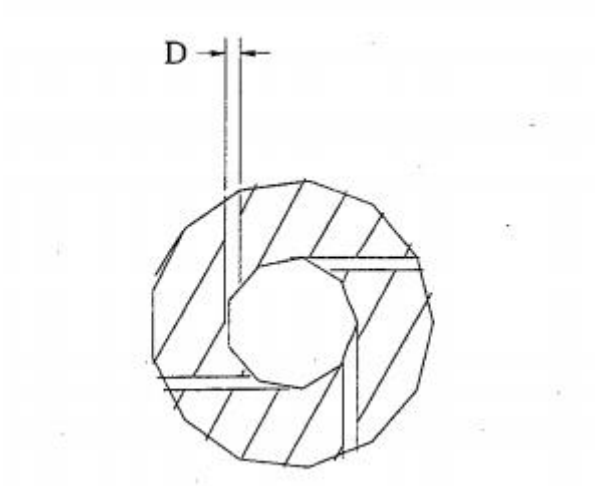

Figure 13 Coaxial swirl injector with 4 tangential ports [20]

To ensure similar characteristics, a non-dimensional parameter was employed that focuses on the mixing capabilities of coaxial swirl injectors. This parameter, the momentum flux ratio, compares the momentum input of both the fuel and oxidizer [26].

$$MFR = \frac{\rho_f V_f^2}{\rho_{ox} V_{ox}^2} \tag{11}$$

This equation shows the Momentum Flux Ratio (MFR) and what parameters are used to determine its value. This parameter was used however, it constrains only the ratio of fuel velocity to oxidizer velocity and thus many solutions exist based on the design criteria. The MFR was found for the proof of concept design to be kept constant for the 1 MW case. The operating pressures as well as fuel and oxidizer types were kept constant resulting in densities being constant and constants in the calculations. The pressure drop requirement thus resulted in a single solution, used for the final design. The diameter was changed for the fuel injection ports to result in a minimum of 20% pressure drop and thus the flow velocity could be found. Using the MFR relation the oxidizer inlet diameter could also be found and implemented.

To find the pressure drop within the injector section was of great concern for combustion stability. The pressure loss is mostly a function of an abrupt contraction through 2.4 mm orifice. The pressure loss is mainly a function of the orifice size and for our case the injection port was assumed to act like an orifice. The pressure loss through an orifice is a common rocket engine design parameter and an approximation was found in the Crane book [27].

$$q = YCA\sqrt{\frac{2\Delta P}{\rho}} \tag{12}$$

Where

$$C = \frac{C_d}{\sqrt{1 - \frac{d_1}{d_2}}} \tag{13}$$

The C and Y values are constants depending on the geometry C is dependent on the manufacturing technique. If the diameter directly upstream to the orifice is sufficiently large, C is equal to C_d. The Y constant is found from the Figure 14.

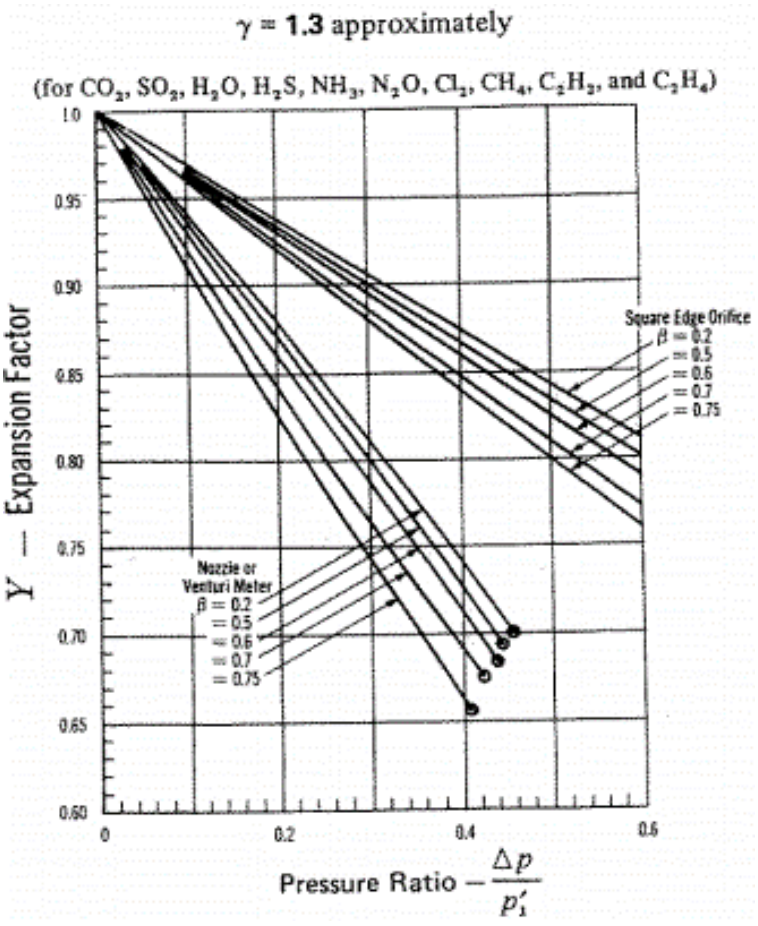

Figure 14 Graph taken from Crane to determine Y the expansion factor [27]

This results in the area, density, and flow rate being the only factors determining the pressure drop. The initial pressure and percent pressure drop are given based on required chamber pressure and combustion stability requirements respectively. The flow rate is set and was decided upon based on required total heat input. Thus the cross sectional area of the orifice is the only parameter that can be manipulated. This allows the orifice diameter to be found assuming a certain requirement for pressure drop.

Deign Parameter Table

Design Criteria	
Power rating	1000 kW
Exit Velocity	2000 m/s
Exit temperature	2800 K
Equivalence ratio	3.5
Combustor material	Inconel 718
Injector	
Tangential Port number	4
Momentum Flux ratio	16
Fuel Pressure drop	20 psi
Injector orifice size	2.8 mm
Combustion Chamber	
Max chamber pressure	101 psi
Characteristic length	1440 mm
Chamber wall thickness	1 mm
Nozzle	
Throat Diameter	16.1 mm
Contraction ratio	7.4
Expansion ratio	1.8
Diverging angle	2°
Converging angle	15°

CHAPTER 3 NUMERICAL METHODOLOGY

3-D CFD COMBUSTION MODEL

The analytical approach described in Chapter 2 was thorough; however, there are many factors and parameters that cannot be found without testing or computational analysis. To help give insight into the design, two main computational models were developed for the 1 MW combustor. Ansys Workbench and Fluent are employed to develop these computational models due to its broad and comprehensive solvers that can be easily linked together. For example, the steady state thermal module can be linked to a static structural module. This software was used to ensure both major sources of stress are represented and simulated, as well as model the combustion characteristics for our unique geometry.

The first solver employed was Fluent to model the combustion process. This helps assess the heat load on the combustor and characterize the exit conditions including temperature and velocity from the combustor. While NASA's Chemical Equilibrium with Applications (CEA) is accurate it is primarily a 1-D code and many of the aspects of our combustor cannot be captured with this software. For example, heat loss to the walls, the mixing effectiveness of the injector, and the velocity distribution of the fluid flow is not captured with a 1-D model. Ansys Fluent can predict the parameters and sources of inaccuracies in CEA discussed above.

The second computational model utilized the thermal stress module which includes both a steady state thermal portion as well as a static structural portion. Fluent results for the heat loss to the wall found from the combustion simulation are used as an input into the steady state thermal model to ensure correct approximation of thermal stress. This allowed for any unknown stress concentrations and inaccuracies of the analytical assumptions to be assessed. The combined stress

solver was also critical in assessing the main mode of failure of the combustor, structural failure due to thermal and mechanical stress, and was used to calculate the combustor factor of safety.

Computational fluid dynamics as well as finite element analysis are both expansive subjects. The exact nature of the simulation and the interworking of the software and its applications are not discussed in this chapter. That can be seen in other works such those as done by Vidana or Aboud [18, 28]. The simulations presented in this thesis are used as a tool to give insight into the details of the design and are compared to the calculations described in Chapter 2.

Governing Equations

Before utilizing the Ansys Fluent software a brief background into its solvers was required. This allowed for a deeper understanding and accurate prediction of the software's limitations. The governing equations are solved using Fluent, this includes the mass and momentum conservation equations, Equations 14-16 [29].

$$\frac{\partial \rho}{\partial t} + \nabla \cdot \left(\rho \vec{V}\right) = 0 \tag{14}$$

$$\frac{\partial}{\partial t}(\rho V) + \nabla \cdot \left(\rho \vec{V}\vec{V}\right) = -\nabla p + \nabla \cdot (\bar{\tau}) + p\vec{g} + \vec{F} \tag{15}$$

Where the $\bar{\tau}$ stress tensor from Equation 15 is shown in Equation 16.

$$\bar{\tau} = \mu\left[\nabla \vec{V} + \nabla \vec{V}^T - \frac{2}{3}\nabla \cdot \vec{V} l\right] \tag{16}$$

Due to the need for mixing as well as modeling of extremely turbulent flows, turbulent models were utilized. The use of the turbulence k-ε model introduces two more sets of equations for that of kinetic energy (k) and dissipation (ϵ) shown in Equations 17 and 18 respectfully [29].

$$\frac{\partial}{\partial t}(\rho \mathcal{K}) + \frac{\partial}{\partial x_i}(\rho \mathcal{K} u_i) = \frac{\partial}{\partial x_j}\left[(\mu + \frac{\mu_t}{\sigma_{\mathcal{K}}})\frac{\partial \mathcal{K}}{\partial x_j}\right] + G_{\mathcal{K}} + G_b - \rho\epsilon - Y_M + S_{\mathcal{K}} \tag{17}$$

$$\frac{\partial}{\partial t}(\rho \epsilon) + \frac{\partial}{\partial x_i}(\rho \epsilon u_i) = \frac{\partial}{\partial x_j}\left[\left(\mu + \frac{\mu_t}{\sigma_\epsilon}\right)\frac{\partial \epsilon}{\partial x_j}\right] + C_{1\epsilon}\frac{\epsilon}{\mathcal{K}}(G_{\mathcal{K}} + C_{3\epsilon}G_b) - C_{2\epsilon}\rho\frac{\epsilon^2}{\mathcal{K}} - S_\epsilon \tag{18}$$

There is also internal combustion occurring within the combustor which can be modeled as a reaction which conserves mass. Ansys can interpret and predict a reaction based on the species produced for a given mass conserving reaction [29]. The species transport Equation must be solved for the combustion reaction of the given fuels and oxidizer. Eq. 19

$$\frac{\partial}{\partial t}(\rho Y_i) + \nabla \cdot (\rho \vec{v} Y_i) = -\nabla \cdot \vec{J}_i + R_i + \mathcal{S}_i \tag{19}$$

The energy equation was also utilized as energy conversion within the combustion model requires the energy model. This simulation required the energy equation to be solved for accurate exit temperatures and thermal stress approximations. The energy equation can be found shown in Eq. 20 [29].

$$\frac{\partial}{\partial t}(\rho \varepsilon) + \nabla \cdot \left(\vec{v}(\rho \varepsilon + \rho)\right) = -\nabla \cdot \left(\sum_j h_j + \mathcal{J}_j\right) + S_h \tag{20}$$

Mesh & Boundary Conditions

The main requirement of the Fluent combustion model of the combustor was to simulate the mixing ability of the injector and ensure the exit parameters were met. This was done by developing a fluid domain and utilizing correct input parameters that would help give insight into such characteristics of the combustor. The exit velocity and exit temperature were design requirements that must be met and validated. The exit velocity requirement is 2000 m/s which for our pressures and chemical composition results in a sonic velocity of around Mach 1.8 and the exit temperature of 2800 K. To ensure that the design meets these requirements the 3D Ansys combustion model was developed and compared to that of the NASA's Chemical Equilibrium with Applications (CEA) results. The CEA input was found using the given inputs.

Table 4 Chemical Equilibrium Analysis (CEA) input parameters for the 1 MW design

Pin	=	101.5	PSIA			
CASE	=	2171043				
REACTANT	WT	FRACTION	ENERGY		TEMP	
(SEE	NOTE)		KJ/KG-MOL		K	
FUEL		CH4	1	-74600	298.15	
OXIDANT		O2	1	0	298.15	
O/F=		3.6266	%FUEL=	21.614129	R,EQ.RATIO=	1.1
Ae/At		1.6				

CEA makes certain assumptions and is limited by a 1-D equilibrium analysis. Ansys software helps to resolve this. Assumptions that CEA utilizes are that the fuel and oxidizer mix perfectly, and complete combustion occurs. These assumptions while accurate for a multitude of cases are unrealistic. One such concern was assessing the degree to which these assumptions affect the exit parameters. The assumption of complete combustion will overestimate the exit temperature. To account for theses specific inaccuracies Ansys was used as a model that more accurately predicts the temperatures and velocities. This computational model was used to assess the assumptions made at the exit of the combustor and also in the optimization of the performance of the combustor.

Ansys Fluent, solves the governing equations and calculates the heat transfer, velocity profiles of a gaseous mixture, and non-premixed combustion temperatures by means of fuel and oxidizer inlet conditions. Ansys Fluent also models combustion and multi-fluid simulations required for our power generation combustor analysis. [29] The fluid domain geometry was imported from NX and a mesh was developed in Ansys meshing tool. The fluid domain geometry used in the software is described in Figures 15– 16.

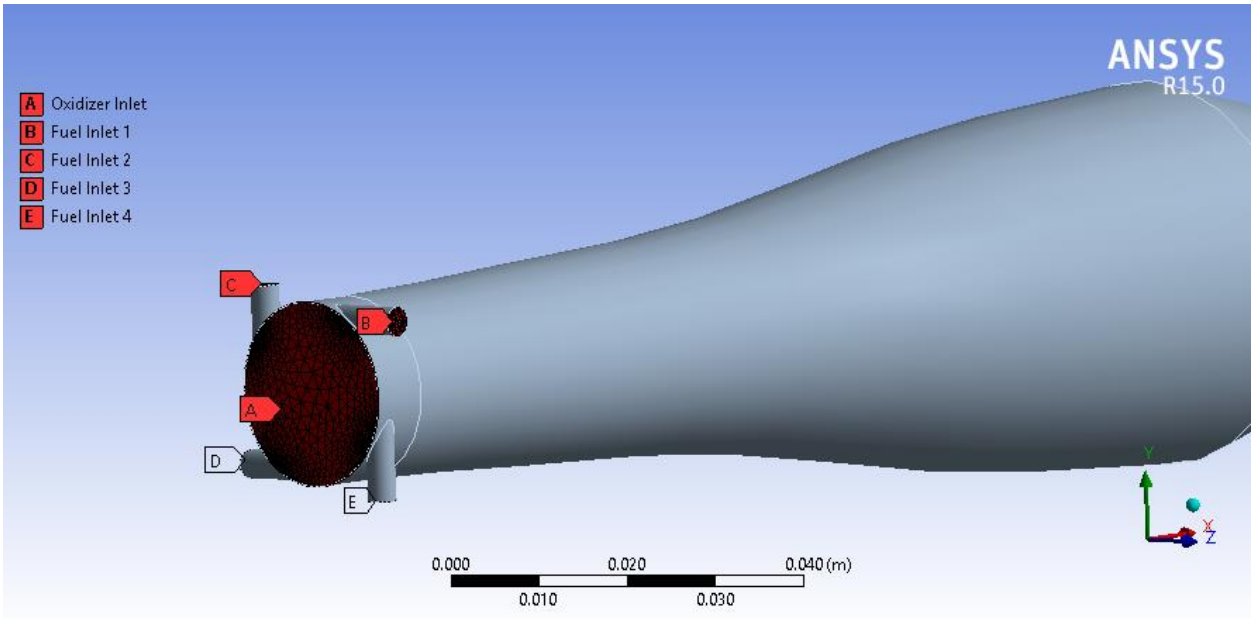

Figure 15 Fuel inlets and oxidizer inlet for the 3D mesh

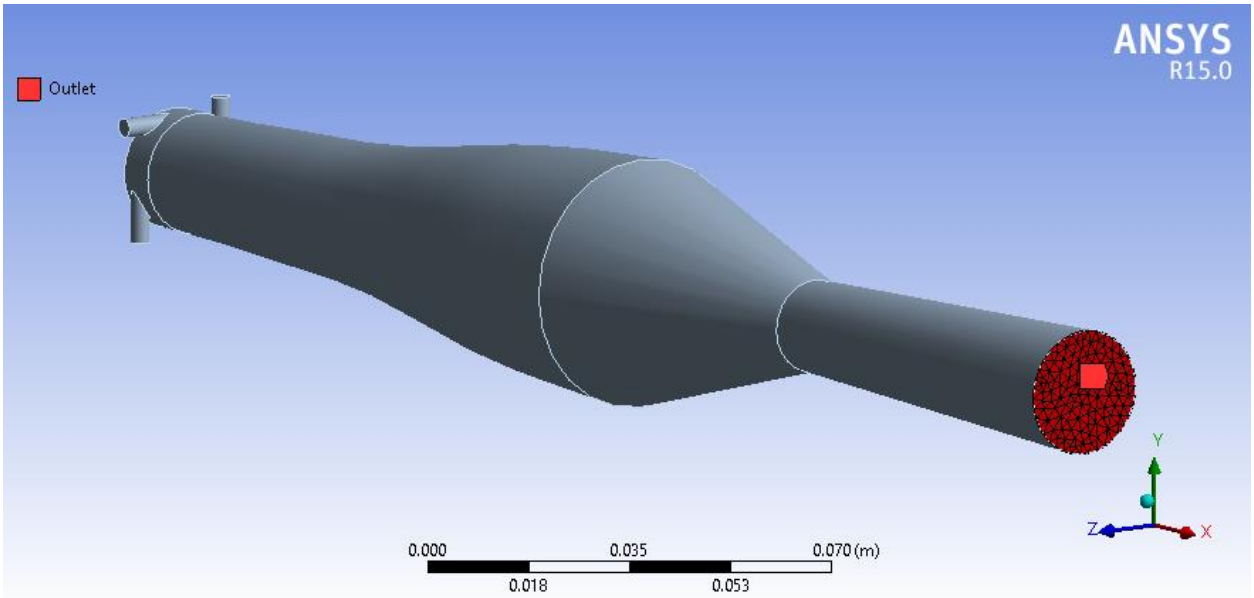

Figure 16 Entire fluid domain showing the outlet from the 3D mesh

The model is essential to solving the mixing capabilities of the combustor and thus multiple inlet conditions were required. While the geometry of the combustor is axially symmetric the resulting combustion process within the combustor is not expected to be symmetric. This is due to the spiral velocity profiles created by the swirl co-axial injector and thus the entire combustor was required to be modeled.

The boundary conditions used in the computational model can be seen in Table 5 shown below. Other components of the input file can be seen in appendix.

Table 5 CFD combustion model input parameters

Models	Energy –On Viscous – Realizable k-epsilon Radiation – P1 Heat Transfer – On Species – Non-premixed combustion • Inlet Diffusion – On • Compressibility Effects – On • Fuel stream reach flammability limit – On • Mass fraction of CH4 – 1 • Mass fraction of O2 - 2
Materials	Fuel – Methane Oxidizer – Oxygen PDF mixture coefficient – wsggm- domain-based
Boundary Conditions	Fuel Inlet: • Mass flow rate – 4.5 g/s per orifice • Hydraulic diameter of 2.8 mm • Mean mixture fraction – 1 Oxidizer Inlet: • Mass flow rate – 65 g/s • Hydraulic diameter – 21.8 mm Outlet: • Hydraulic diameter – 25 mm
Solution Initialization	Standard – Oxidizer Inlet

To ensure that the model was accurate the mesh was refined and then compared with the analytical approach until refinement resulted in no significant change in error between the different grid sizes. This was found to be at the element number of 220,000.

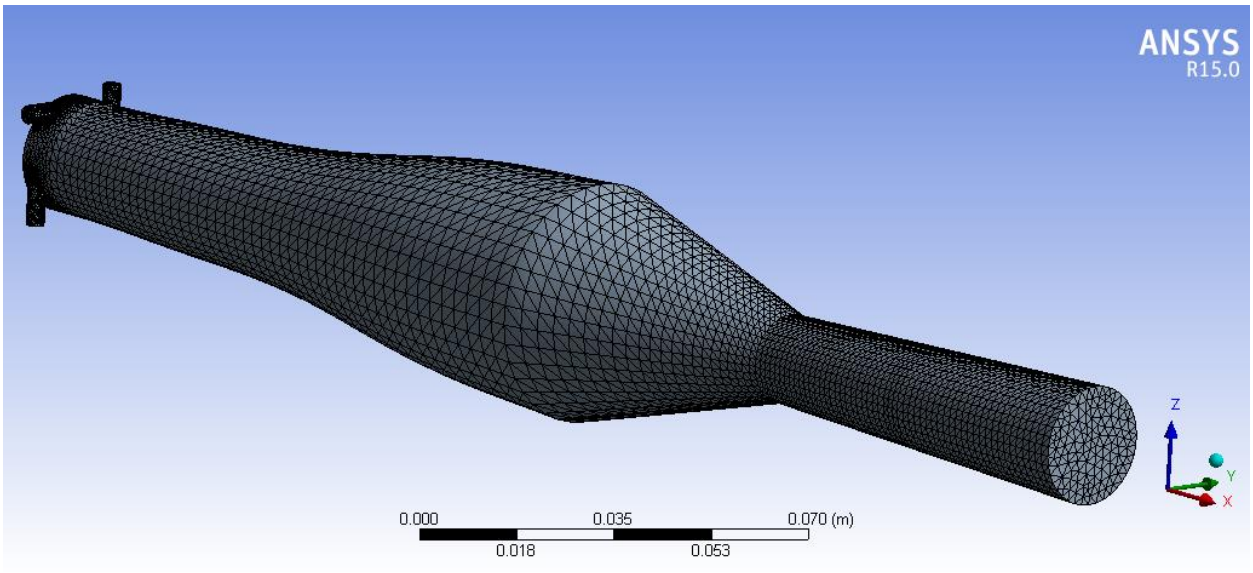

Figure 17 Mesh generated for CFD combustion of a 1 MW system

The geometry has a cylindrically structured mesh consisting of 220,000 tetrahedral elements. Ninety-five percent of the elements are above 0.6 orthogonal quality, with an average of 0.83, and an average aspect ratio of 1.9. A refinement also occurred for the lowest quality elements to raise the minimum orthogonal quality to 0.35 to ensure the elimination of errors due to mesh quality.

FEA MODEL

The second chapter of this thesis presented a 1-D approximation for the stress at the throat. This stress approximation is made specifically for a rocket engine with cooling channels. However, our geometry is complex and could allow for unforeseen stress concentrations. Validation of the value is critical to the longevity of the combustor and assessing the main mode of failure of the design. These reasons lead to a 3-D finite element analysis to be developed to gain more details than the 1-D model could provide. The finite element model accounts for both the thermal stress and structural stress seen in the combustion chamber similar to that of the 1-D analytical approach. This was done by developing a steady state thermal model to output a 3-D temperature profile that was then inputted into the static structural model of Ansys. The 3-D combustion model resulted in a heat flux to the outer wall of the combustor. This was inputted to the steady state thermal model along with an overall heat transfer coefficient from the expected water flow calculation. This allowed the steady thermal model to produce a 3-D thermal profile of the combustor under hot fire combustion and water cooling conditions. This thermal profile along with fluid pressure conditions and fixed wall boundary conditions in the static structural model could produce an accurate combined stress result.

A rough combined steady state and static structural model was developed for the entire combustor, to ensure that the highest combined stress was located near the throat. The model showed that the highest stress concentration was at the throat and no other sources of stress concentrations were found. However, modeling the entire combustor was inaccurate as compared to the analytical results. This was shown when increasing element count to the limitation was still overestimating the highest stress by 40%. This lead to a more concentrated simulation, with refinement near the throat, modeling only the converging and diverging section of the combustor. This was then refined and compared to the analytical approach. The refined partial model showed accurate prediction of the stress within 10% and thus was the main focus for safety considerations.

Mesh & Boundary Conditions

The combined stress model was developed modeling the combustor walls surrounding the combustion gases. This model was the basis for the safety factor and cooling requirements for the direct power extraction system, namely the stress at the throat. The boundary conditions were centered on the stress approximation of the throat. The model was that of the material wall of the combustor strictly including the converging and diverging section. The steady state thermal model utilized the critical aspects of the thermodynamic process, namely the cooling channels and combustion chamber inner wall.

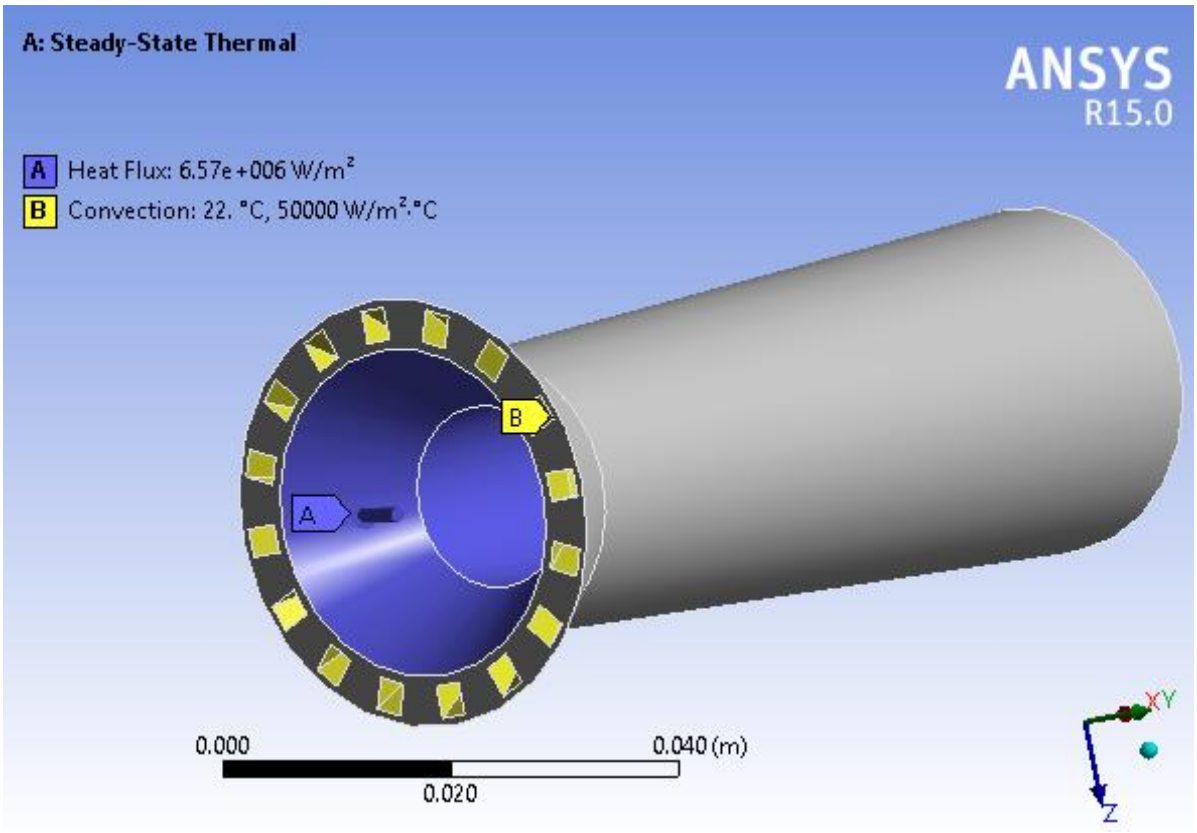

Figure 18 Geometry and boundary interfaces for the steady state thermal model

A heat flux found from the combustion model was utilized to represent the combustion process for this inner wall boundary condition on the blue face (A) in Figure 18. The cooling channel water flow was represented by the analytical result of overall cooling coefficient value for

the expected water flow parameters on the yellow faces (B) in Figure 18. The model developed as well as the faces utilized for the steady state thermal model can be seen in Figure 18.

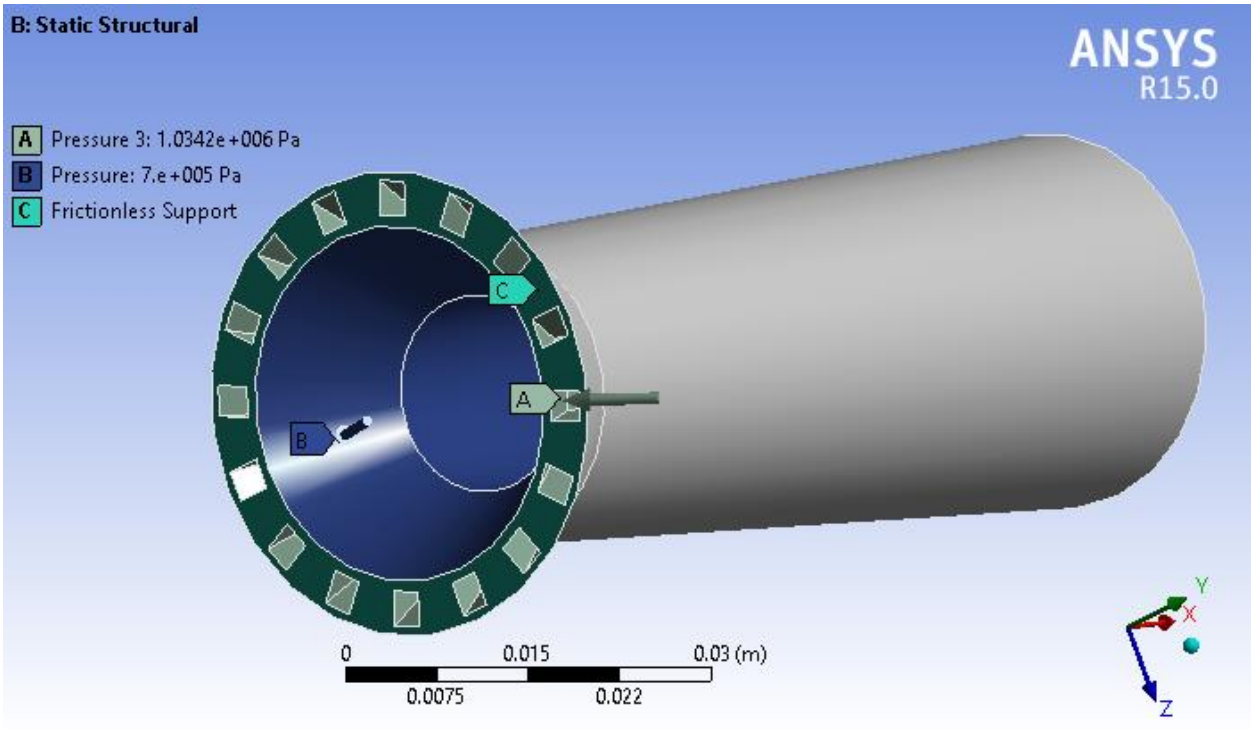

Figure 19 Geometry and boundary interfaces for the static structural model

The static structural model employed the same geometry however the face highlighted in green (C) in Figure 19 was used as the frictionless support. This face is where the rest of the combustor would be located. The combustor will be supported on the injector side and thus must be supported from the upstream portion. The pressure aspect of the fluids were applied to the respective faces of the combustor inner wall (B) and cooling channels (A) in Figure 19. The combined stress model input parameters can be seen below in Table 6.

Table 6 Combined stress model input parameters

Models	Steady state thermal • Heat flux • Overall heat transfer coefficient Static Structural • Pressure • Frictionless supports
Materials	Inconel 718
Boundary Conditions	Combustion inner chamber wall: • Heat flux out – 6.57 MW/m^2 • Chamber pressure – 101 psi Cooling channel: • Overall Heat transfer coefficient – 50,000 W/m^2k each • Water Pressure – 150 psi
Output	Von Mises stress – On

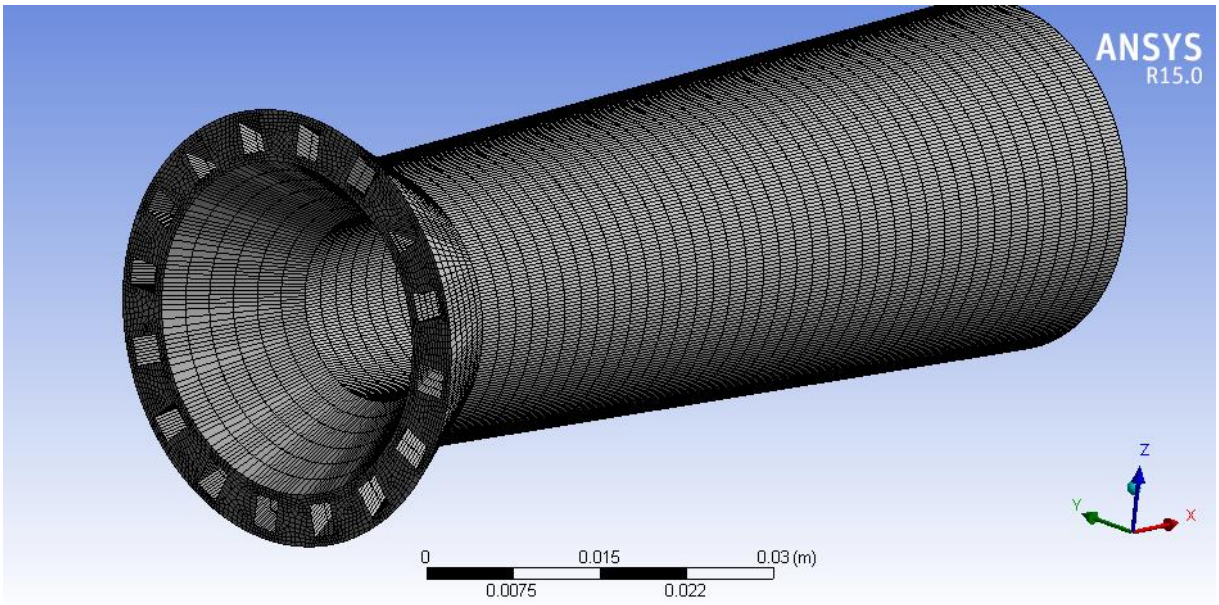

Figure 20 Mesh used for the FEA model

A proper mesh was required for accurate results of the combined stress model. The mesh was made using the sweep method and used edge sizing to ensure a minimum quality was met at specified locations. The edge sizing was used to ensure enough elements were utilized to segment the cooling channels and the 1 mm wall material between the channels and the inner combustor wall. This wall between these two regions is where the highest stress is shown to occur and thus a point of great interest. The elements used were hexahedral, with an amount of 120,000. The element quality given by the Ansys meshing tool was a 0.5 average with a 0.3 minimum.

CHAPTER 4: RESULTS AND DISCUSSION

3-D CFD COMBUSTION MODEL

Velocity Contours

After simulating many designs, the final design was chosen below. One unforeseen parameter that greatly affected the combustion process was velocity distribution, discussed in the next section. In terms of exit temperatures, little difference is observed between NASA CEA and the 3D combustion model.

Table 7 Exit velocity comparison between the two method employed

Velocity	CEA	ANSYS	% Error
	1980	1960	1.5

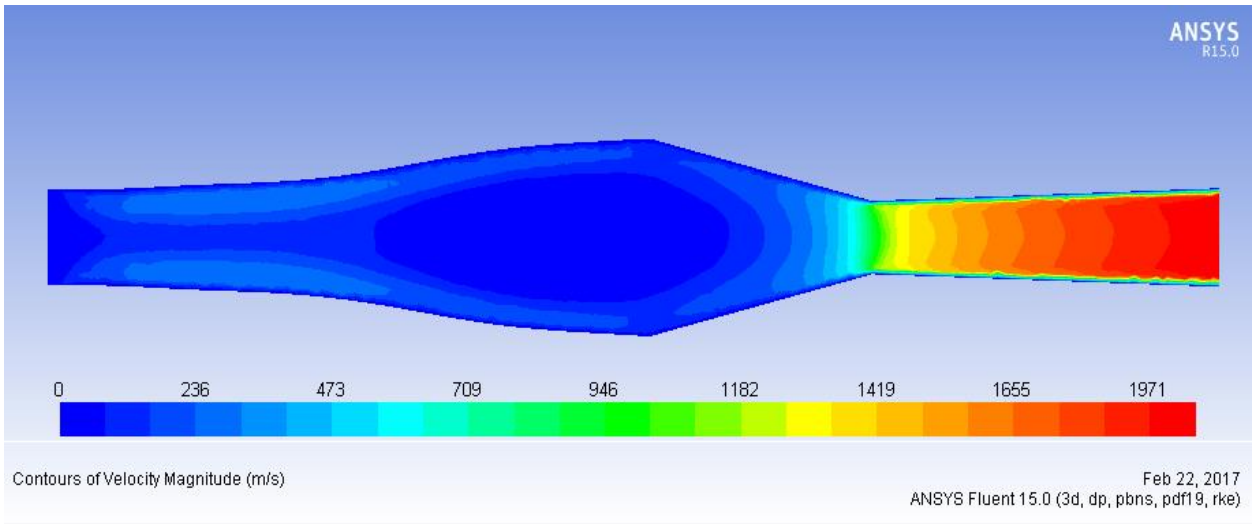

Figure 21 Velocity absolute magnitude of the fluid within the combustion chamber

Figure 21 presents a velocity contour of an axial cross section of the 3-D combustion model. As the results indicate the values were lower than that predicted by CEA. Though there was a decrease from the 1-D approach in exit velocity the accuracy and amount suggests that this design is sufficient for meeting the design requirements. While there was a sufficient inner core of the exit gases meeting the 1980 m/s condition there was a boundary layer effect which slowed the overall average velocity to the 1960 m/s near the wall. This accuracy suggests agreement between the analytical approach as well as correct application of NASA CEA and Ansys fluent. Both software predicts speeds at the throat when compared to CEA as well as the correct Mach number equal to one. Here it can be seen that the initial high velocity region for the mixing works as intended. The methane, has a velocity five times faster than the oxidizer due to the smaller diameter of the tangential ports, swirls in a direction tangential to the post and creates an intense mixing zone with the oxidizer.

Transition Region

The injector design process resulted in an oxidizer inlet ~50% that the of the combustion chamber diameter. This requires a transition from oxidizer inlet to chamber diameter, of which the initial design did not include, discussed in the beginning of Chapter 2. The transitions considered were that of a step, 5° half angle diffusor, 15° half angle diffusor, as well as a specialized 5th order polynomial, (A),(B),(C), and (D) respectfully. [30]

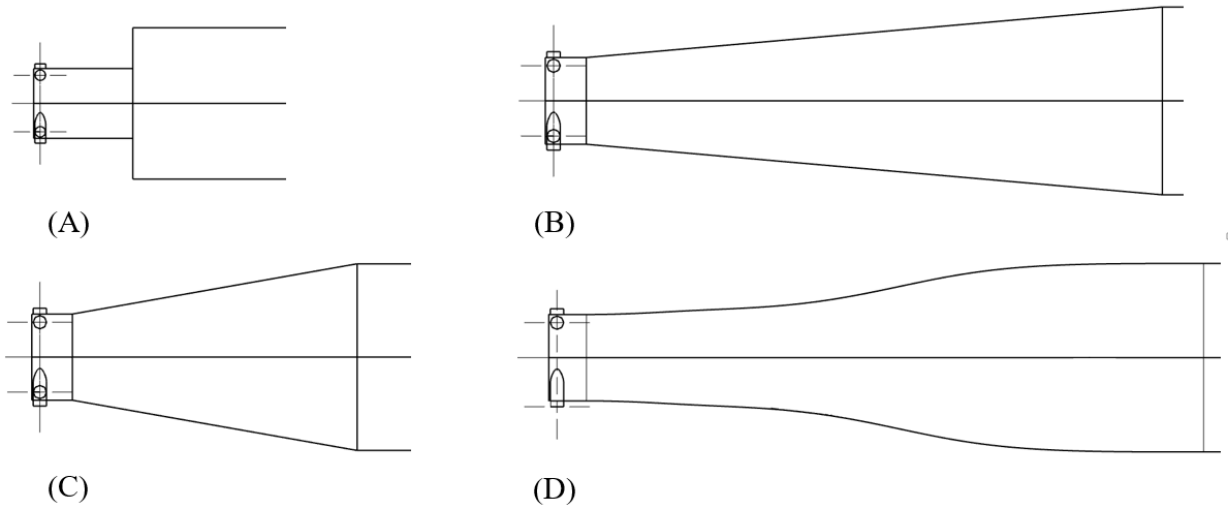

Figure 22 All types of transition geometries considered and modeled for the 1 MW combustion chamber

The 5th order polynomial was decided upon when considering required velocity characteristics and indications of complete combustion. This polynomial was found solving the boundary flow equations while generating a uniform velocity profile at its outlet [30]. The profile used for the inlet section is shown in Eq. 21 and was modified for the change in diameters for the specific transition related to the current combustor.

$$r(L) = -0.00926\,L^5 + 0.0694\,L^4 - 0.1389\,L^3 + 0.5 \qquad (21)$$

These results were found conducting a 3D combustion simulation on each design in Ansys Fluent. The transitions from the oxidizer inlet to the combustion chamber exhibited issues for chamber velocities as well as mass fractions of O_2. It was observed that O_2 was seen in high concentrations >20% throughout the majority (70% of the length) of the combustion chamber. High concentrations of oxygen in downstream sections of the combustion chamber suggests poor mixing, which can result in incomplete combustion. The comparison of the O_2 concentration can be seen in Figure 23. The velocity was also seen to be high (Mach 0.5) within the oxidizer section for the simple step configuration, or the abrupt diffusor (A) and (C) in Figure 22. The 5th order polynomial was derived to provide an equal velocity profile in the radial direction [30]. Thus, this 5th order polynomial was implemented to distribute the velocity more evenly to reduce the high velocity region. It was seen that when distributing the velocity, the region of high oxygen concentration was reduced by around 30%. The velocity being distributed more towards the edges resulted in lower velocity maximums from Mach 0.5 to Mach 0.3

One crucial aspect of the CFD combustion model was assessing the mixing capability and combustion efficiency of the design. It was assumed that if the initial conditions are keep constant and a change in geometry led to a reduction in O_2 fraction volume, better mixing occurred. This is due to how Ansys determines if combustion occurs. Ansys 15 specifically assumes that if a gaseous mixture of fuel and oxidizer are sufficiently mixed, they will combust. A reduction in O_2 or methane concentration indicates enhanced mixing. The 5th order polynomial found from literature only focuses on distributing velocity equally during a change in cross sectional area. However, results suggest this led to better mixing, as achieving an evenly distributed velocity. The volume of the combustion chamber with less than 10% O_2 was reduced from occupying 70% of the length with the conical transition to near 40% of the length with the 5th order polynomial as can be seen in Figure 23.

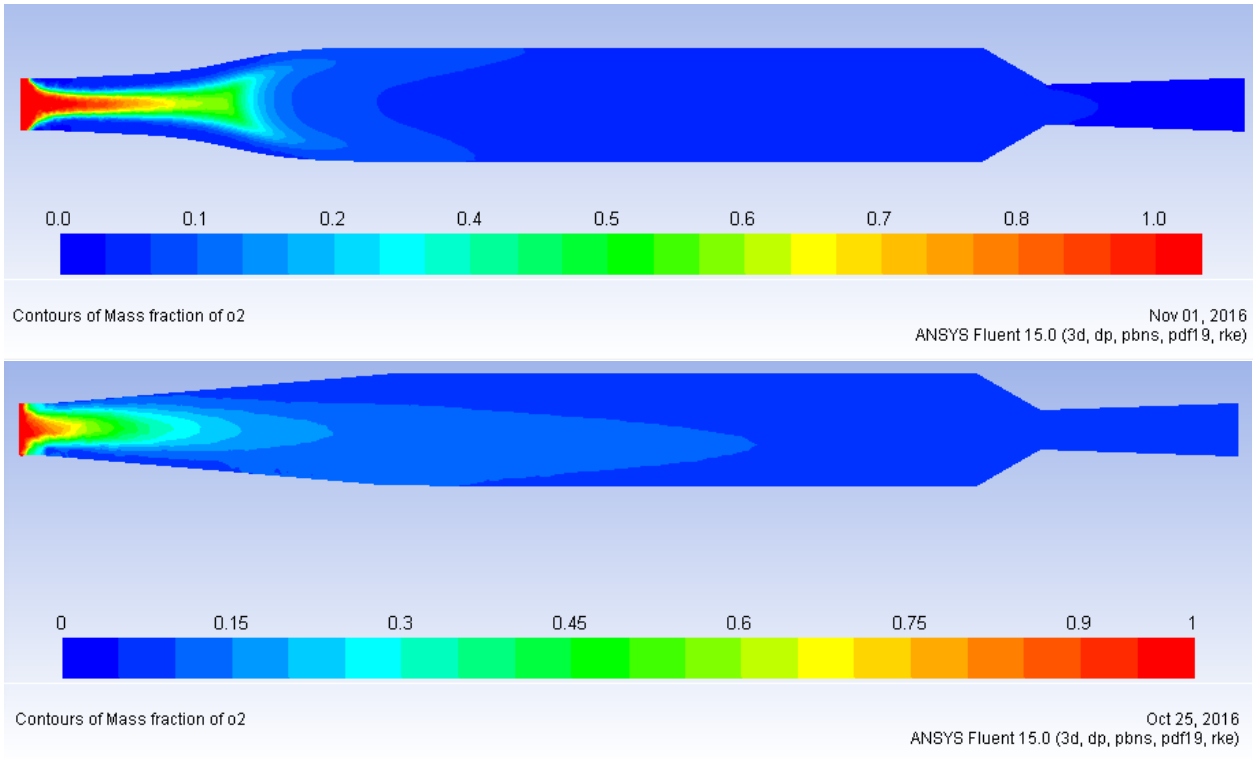

Figure 23 Oxygen mass fraction of both conical and 5th order polynomial geometries during steady state combustion

This along with initial temperature profiles indicated that the combustion chamber length could be reduced, which literature confirms [17]. This along with the exit parameters being met led to the reduction in length of the combustor. The improved mixing between the 5^{th} order and the other transitions could be due to more oxygen being distributed to the edges where the swirling methane is located. This would be forcing the methane and oxygen to interact resulting in better mixing. The 5^{th} order polynomial is designed to distribute the center flow to the edges which could case this enhanced mixing. The fraction of O_2 suggests this conclusion. One could note the lack of symmetry in the results. This suggests that a refinement of the mesh is required however computational time was exceeding reasonable amounts for very minimal increases in accuracy. All other aspects of the results suggest sufficient accuracy was met such as the velocity profiles and exit parameters. One other aspect of the design was that led to asymmetric results was that the mesh was not perfectly symmetrical.

Temperature Contours

Exit temperature differs from the 1-D analytical approach. The 3D combustion model can help analyze many of the assumptions made during the analytical approach. This Ansys simulation can predict average exit temperature to account for the losses discussed for the exit velocity. This results in very similar results to the CEA approximation. The percent error is greater for the exit temperature as compared to the exit velocity. However, it is still considered acceptable for the final design. This could suggest a decrease in diverging length, which increases temperature, however for this design stage 2.7% error was deemed sufficient.

Table 8 Exit Temperature Comparison between the 1-D and 3-D models

	CEA	Ansys	Error
Temperature	2920 K	2840 K	2.7 %

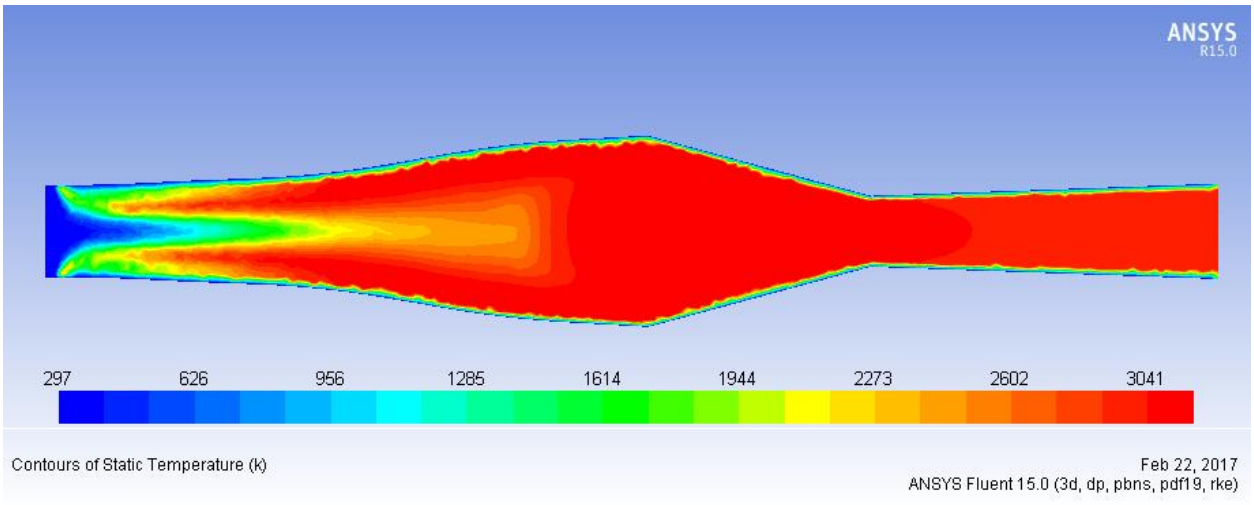

Figure 24 Temperature contour of the 1 MW design during steady state operation

Figure 24 is a temperature contour of a cross section of the 3-D combustion model. The exit temperature reaches the required 2800 K goal set from the design requirements. The temperature near the injector face can be seen to be higher near the wall, as this is where a majority of mixing occurs. This can due to the swirl injector causes higher velocity and thus better mixing in this region. The temperature reaches a maximum towards the end of the transition region, which is desired as an earlier would suggest a reduction in length.

FEA MODEL

Stress and Stress Concentrations

The thermal stress of the combustor was determined to be the most critical parameter in terms of safety for our design. This alongside the cooling capability are of the utmost concern in terms of safety design. This is due to correct prediction of the thermal stress only being possible with accurate cooling approximation. Though the stress at the throat was known to be the maximum for the design of the combustor, the entire combustor was initially modeled. This was to ensure any modifications, such as the transition region between the injector and combustion chamber, would not have any unforeseen effects on the stress predictions. Once the initial model confirmed the assumption that the throat was indeed the location of the maximum stress, a more refined model focusing on the throat section was implemented. This final model only considered the converging and diverging section of the combustor to allow for finer elements to be used, as the element amount was limited. This refined model resulted in predictions within 2 percent error to the combined stress equation.

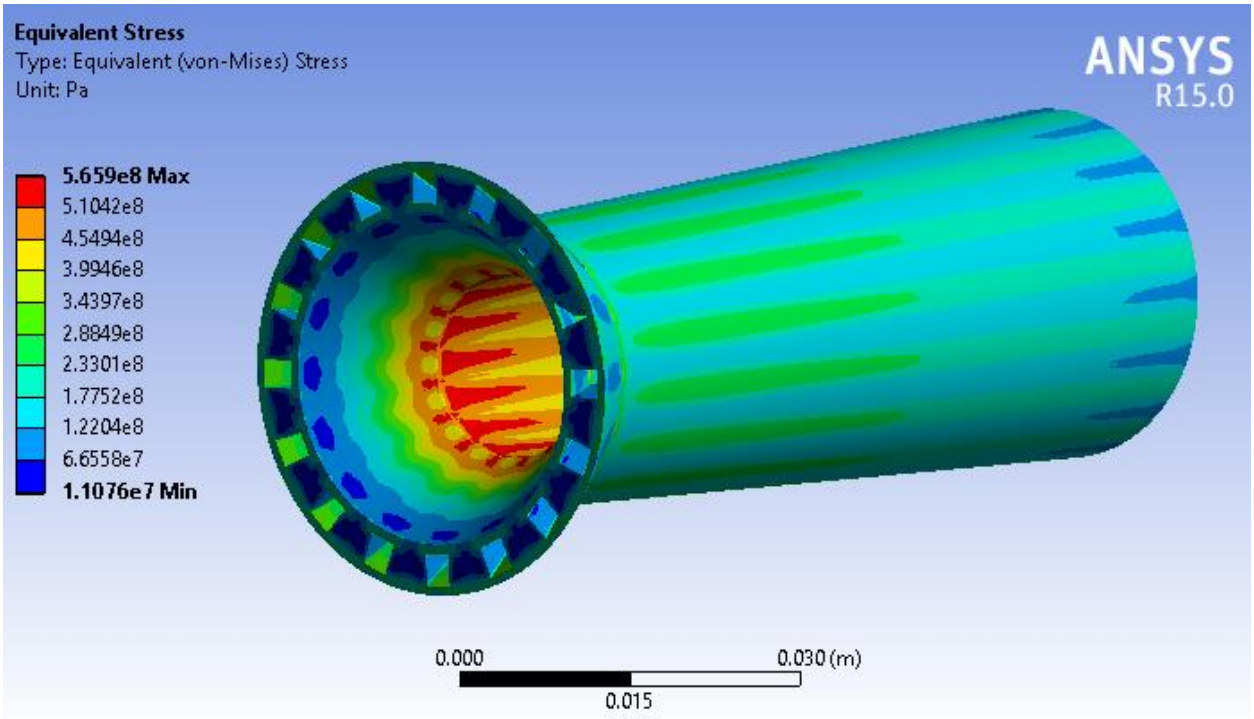

Figure 25 Von Mises combined stress result

The stress shows that of the predicted characteristics show an increase in stress reaching a maximum at the throat and slowly decreasing downstream. The stress was also highest where the highest thermal gradients were located, i.e. location of the cooling channels. This can be seen as a stripped formation along the inner walls of the combustor in Figure 24. The highest value determined from our final combined stress model was that of 566 MPa, Figure 24.

To ensure the maximum possible stress was predicted through our computational model many conservative values were utilized for the input parameters. The conservative values include implementing the predicted heat flux at the throat from Bartz correlation as the inner wall boundary condition. A literature review as well as thermal profile analysis conducted suggests

that Bartz correlation over predicts the heat flux exiting the chamber wall [31]. This value of the actual heat flux typically found to be 60% of the value predicted by Bartz correlation. The stress was predicted from the theoretical approach described in Chapter 2 to be 570 MPa. Another conservative measure was assuming the limit of the material, Inconel 718, at the highest expected temperature of 600°C. The yield strength of Inconel 718 at 600°C is in 1000 MPa. If considering the heat flux modified from Bartz correlation (including a 40% reduction) the factor of safety increases to 1.75 and comes within the 2% error of the analytical approach. A source from NASA had specifications for a rocket engine combustion chamber factor of safety. The NASA report considered a factor of safety of at least 1.4 to pass certain regulations [32]. Due to the higher factor of safety by 30% and a conservative approach for both the cooling system as well as material properties, the system passed stipulations to continue to production.

CHAPTER 5: SUMMARY AND CONCLUSIONS

EXPECTED PERFORMANCE

To assess the design validity of the combustor the values generated by different methods were compared to both each other as well as the values generated from the 60 kW design methodology and experimental data. This includes the prediction of the crucial required parameters of the exit gas conditions as well as thermal stresses. This along with the combustion efficiency of the nozzle, the comparison to the initial proof of concept design and the thermal stress analysis leads to the high confidence validity of the design. First we shall consider the exit gas properties.

The NASA CEA software along with the parameters taken from the previous design as inputs led to the relative high accuracy for these conditions. The exit velocity was found to result in 1980 m/s at the expansion ratio given however neglects the slowing of the fluid do to viscous losses as well as expansion efficiency. The issue of validation of these losses was solved via the usage of ANSYS CFD non-premixed combustion simulation as well as compressible fluid dynamic solvers. This led to a 3-D model of the working fluids after injection, modeling of the mixture process as well as solving of exit parameters. Much of the work was initial developed during the evaluation for the proof of concept design by Vidaña [18]. This lead to the Ansys result of 1960 m/s for the exit velocity. This results in an underestimation of -1.5% error from the CEA approach and -4% error for the 2000 m/s requirement. This is likely is a result of the effects slowing the flow such as boundary layer effects and other viscous losses not modeled within the 1-D approach. However, a maximization of the nozzle expansion efficiency (99%) allowed for the average exit velocity to be within 5% error of the required value. The acceptable limit for the error for this design requirement was ±10% meaning the design passed the requirements criteria. The exit temperature followed a very similar path in terms of comparison with CEA. Initially CEA was used as a broad solver with Ansys validation refining the design choices. This lead a CEA result of 2920 K for exit temperature considerably higher than the 2800K requirement. The CEA

software leads to inaccuracies lack of accounting for incomplete combustion. The large overestimation was due to anticipation of the losses discussed above as learned from the 60 kW design process. The Ansys software led to an exit velocity of 2840 K, which results in -2.7% error from the CEA value however also results in +1% error from the design requirement of 2800 K. This was due to overshooting of the 1-D results to account for the losses.

The geometry of the transition region between that of the injector face to the combustion chamber shown to effect combustor performance significantly during initial combustion simulations. The optimizing of the transition region led to a reduction in length which in turn increases the exit temperature when compared to the oversized combustion chamber length. This is due to better mixing capabilities of the design by inclusion of a more radially distributed velocity.

The injector was held to strict guidelines for expected performance changes. A 20% pressure drop was required to restrict combustion pressure variations to effect the feed lines upstream and thus reduce combustion instability. The successful coaxial swirl injector used in the 60 kW combustor was scaled utilizing scaling parameters to match mixing capabilities. Such scaling parameters included the momentum flux ratio to mimic performance. The results presented in the velocity contours of the 3-D combustion simulation suggests adequate mixing and performance.

The next criteria of comparison was that of the combined stress within the combustor wall. The stress specifically at the throat was used for safety concerns and correct approximation of this value validated cooling parameters developed. A steady state thermal model using the values developed in the cooling parameter section of the design methodology were used to develop a 3-D temperature profile of the combustor wall. This was inputted into a static structural model of the combustor wall that can output the stresses developed under firing conditions. The stress at the

throat was compared to that predicted by the combined stress section of the design methodology to ensure combustor structural integrity. The value of the theoretical analysis predicted a maximum stress of 570 MPa at the throat. The combined model developed in Ansys resulted in a maximum stress at the throat of 565 MPa near 1% error to that of the theoretical approach. This results in a Factor of safety of 1.7 when considering the material properties of Inconel 718 at the highest temperature expected of 650°C. This Factor of Safety is well above those typically considered for similar combustion devices and was confirmed by similar values obtained from the 60 kW combustor.

NEXT STEP/CONSIDERATIONS

The achievement of designing and successfully testing a super alloy pure oxygen hydrocarbon combustor for extended periods strengthens the argument for a revival in direct power extraction. The utilization of a super alloy as well as cooling channels within the walls allows for the higher flame temperatures desired while also minimizing the heat loss to the wall. The data obtained from the 60 kW combustor tests supports this claim and would result in an increase in thermodynamic efficiency. The development of the 1 MW version allows for next steps to be taken for implementation in full scaled models. This type of device as a topping system in current thermal power plants would allow for rapid and relatively cheap changes to the existing systems that can also fully utilize pure oxygen based combustion. The understanding of proper scaling for direct power extraction system would lead to rapid growth for implementation of topping systems for a variety of power generation applications. The utilization of oxy-combustion would allow for the critical temperature range needed for ionization within MHD systems, namely the 2700 K range and higher. The utilization of super alloy combustor material as well as computational analysis for thermal management could greatly increase the maximum temperature achievable without

dropping the safety. Once proper scaling and data validates the oxy-fuel based super alloy direct power extraction system, implementation would result in drastic increases in efficiency and emission reduction.

REFERENCES

[1] U.S. Energy Information Administration, "Annual Energy Outlook 2017 with projection to 2050," U.S. Energy Information Administration, 2017.

[2] UNFCCC. Conference of the Parties (COP), "Adoption of the Paris Agreement. Proposal by the President.," Paris, 2015.

[3] U. D. o. Energy, DOE Fundamentals handbook Nuclear physics and reactor theory Volume 1 of 2, Washingtion D.C: U.S. Department of Energy, 1993.

[4] U. E. P. Agency, "Inventory of U.S. Greenhouse Gas Emissions and Sinks: 1990-2013," National Service Center for Environmental Publications, Washington DC, 2015.

[5] T. Ochs, R. Woodside, D. Oryschchyn and L. Kolczynski, "Improvements in Exergetic Efficiency in High-Temperature Oxyfuel," National Energy Technology Laboratory-In-house Research, 2014.

[6] N. Kayukawa, "Open-cycle magnetohydrodynamic electrical power generation:," *Progress in Energy and Combustion Science,* vol. 30, pp. 33-60, 2004.

[7] S. Way and R. Hundstad, "Direct generation of power from a combustion gas stream," in *Eighth Symposium (International) on Combustion*, Pasadenia, 1961.

[8] J. Nichol, V. Siminski and H. Wolfhard, "Ionization in rocket flames," in *Eighth Symposium (International) on Combustion*, Pasadenia, 1961.

[9] R. C. Murray and e. al., "Observation of MHD Effects with Non-Equilibrium," in *42nd AIAA Aerospace Sciences Meeting and Exhibit*, Reno, 2004.

[10] J. Teno, T. Brogan, S. Petty and e. al., "Research studies and the development of MHD generators and accelerators," AVCO Everett Research Laboratory, Arnold Air Force Base , 1970.

[11] R. Niemann and e. al., "Superconducting magnet system U-25 MHD facility," *IEEE Trmsactions on Magnetics,* vol. 13, no. 1, pp. 632-635, 1977.

[12] M. Mitcher and C. H. Kruger Jr., Partially Ionized Gases, Stanford: John Wilsey & Sons, Inc., 1973.

[13] P. J. Lee and B. Strauss, "Nb-Ti - from beginnings to perfection.," CRC Press, Leiden, 2011.

[14] P. M. Shumyatsky, "U.S./U.S.S.R. Cooperative program in open-cycle MHD electrical power generation," Argonne, 1978.

[15] D. K. Huzel and D. H. Huang, Modern Engineering for design of liquid-propellent rocket engines, Washington DC: American Institute of Aeronautics and Astronautics, 1992.

[16] T. R. Brogan, J. F. Louis, R. J. Rosa and Z. J. J. Stekly, "A review of recent MHD generatio work at the Avco-Evereet Research Laboratory," in *Third Symposium on the engineering aspects of Magnetohydrodynamics*, Evertt, 1962.

[17] J. R. Hulka, "Scaling of Performace in Liquid Propellant Rocket Engine Combustion Devices," in *44th AIAA/ASME/SAE/ASEE Joint Propulsion Conference & Exhibit*, Hartford, 2088.

[18] O. D. Vidaña, M. Chaidez, B. Lovich, A. Jad, M. J. Hernandez, L. A. Cabrera, A. Choudhuri and N. D. Love, "Component and System Modeling of a Direct Power," in *54th AIAA Aersopace Science Meeting*, San Diego, 2016.

[19] M. J. Hernandez, L. Cabrera, O. D. Vidaña, M. Chaidez, A. Choudhuri and N. D. Love, "A Systematic Framework for the Design of an Open-Cycle Direct Power Extraction Combustion-Chamber," in *54th AIAA Aerospace Sciences Meeting*, San Diego, 2016 .

[20] M. R. Long, V. G. Bazarov and W. E. Anderson, "Main chamber injectors for advanced hydrocarbon booster engines," in *39th AIAA/ASME/SAE/ASEE Joint Propulsion Conference and Exhibit* , Huntsville, 2003.

[21] L. A. Cabrera, J. Aboud, M. J. Hernandez and e. al, "Heat Transfer Characterization of a High Heat Flux Oxy-Fuel Direct Power Extraction Combustor," in *55th AIAA Aerospace Sciences Meeting* , Grapevine, 2017.

[22] S. R. Turns, Introduction to Combustion 2nd edition, Singapore: McGraw-Hill Book Co, 2000.

[23] C. H. Negus, An Interactive Chemical Equilibrium Solver for the Personal Computer, Blacksburg: Faculty of the Virginia Polytechnic Institute and State University, 1997.

[24] C. A. Synder, "CEARUN," 7 May 2004. [Online]. Available: https://cearun.grc.nasa.gov/.

[25] Y. A. Çengel and J. M. Cimbala, Fluid Mechanics, New York: McGraw-Hill, 2006.

[26] M. R. Long, V. G. Bazarov and W. E. Anderson, "Main chamber injectors for advanced hydrocarbon booster engines," in *39th AIAAlASMElSAElASEE Joint Propulsion Conference a'1d Exhibit* , Huntsville, 2003.

[27] Crane Co., Flow of fluids through valves, fittings, and pipe, Chicago: Crane Co., 1965.

[28] J. G. Aboud, *Design of a thermal management system for an oxy-methane direct power extraction combustor,* El Paso: University of Texas at El Paso, 2016.

[29] ANSYS, Inc., *ANSYS Fluent Theory Guide,* Canonsburg: ANSYS, 2013.

[30] M. Subramanya, D. S. Davu and A. Choudhuri, "Experimental Investigation on the Flame Extinction Limit of Fuel Blends," in *43rd AIAA Aerospace Sciences Meeting and Exhibit*, El Paso, 2005.

[31] D. M. Smith, *A comparison of experimental heat-transfer coefficients in a nozzle with analytical predictions from Bart's methods for various combustion chamber pressures in a solid propellent rocket motor,* Raleigh: North Caroline State University at Raleigh Department of Mechanical and Aerospace engineering, 1970.

[32] K. S. Bernstein, "Structural Design Requirements and Factors of Safety for Spaceflight Hardware For Human Spaceflight," National Aeronautics and Space Administration Lyndon B. Johnson Space Center, Houston, 2011.

[33] M. General Editors Petrick and B. Y. Shumyatsky, Open-Cycle Magnetohydrodynamic Electrical Power Generations, Argonne: Argonne National Laboratory, 1978.

APPENDIX

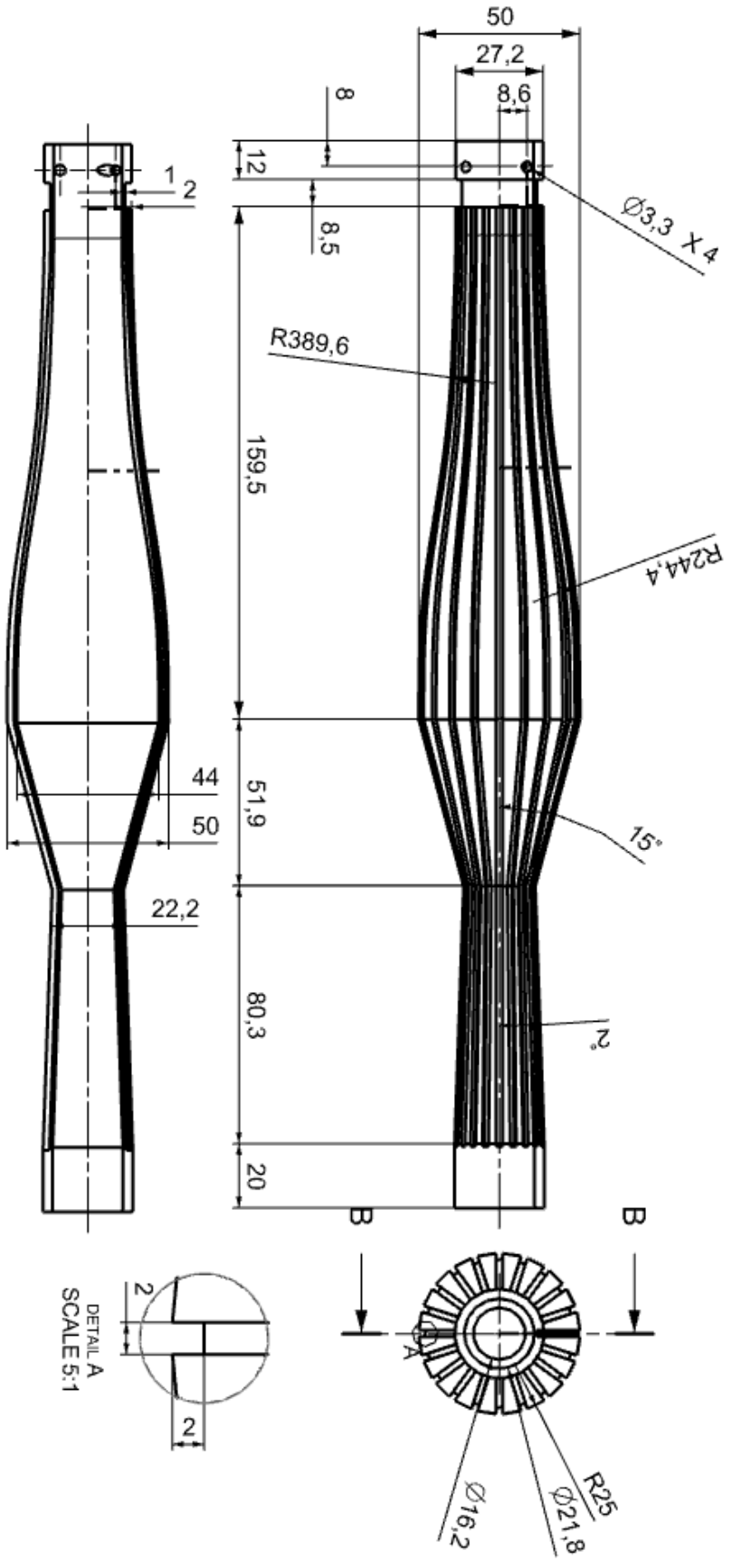
50
27,2
8,6
8
12
8,5
1
2
Ø3,3 X 4
R389,6
159,5
R244,4
44
50
51,9
15°
22,2
80,3
2°
20
B
B
DETAIL A
SCALE 5:1
2
2
A
Ø16,2
R25
Ø21,8

Fluent

Version: 3d, dp, pbns, pdf19, rke (3d, double precision, pressure-based, 19 species pdf, realizable k-epsilon)

Release: 15.0.7

Title:

Models

Model	Settings
Space	3D
Time	Steady
Viscous	Realizable k-epsilon turbulence model
Wall Treatment	Standard Wall Functions
Heat Transfer	Enabled
Radiation	P1 Model
Species	Non-Premixed Combustion ((ch4 o2 ch2o cho co co2 h h2 h2o h2o2 hco hcooh ho2 hoco o oh o3 c oc<oh>2) species)
Coupled Dispersed Phase	Disabled
NOx Pollutants	Disabled
SOx Pollutants	Disabled
Soot	Disabled
Mercury Pollutants	Disabled

Material Properties

Material: pdf-mixture (mixture)

Property	Units	Method	Value(s)

Mixture Species names (ch4 o2 ch2o cho co co2 h h2 h2o h2o2 hco hcooh ho2 hoco o oh o3 c oc<oh>2)

Density kg/m3 pdf #f

Cp (Specific Heat) j/kg-k mixing-law #f

Thermal Conductivity w/m-k constant 0.0454

Viscosity kg/m-s constant 1.72e-05

Absorption Coefficient 1/m constant 0

Scattering Coefficient 1/m constant 0

Scattering Phase Function isotropic #f

Refractive Index constant 1

Speed of Sound m/s none #f

Material: (o2 . pdf-mixture) (fluid)

Property	Units	Method	Value(s)
Density	kg/m3	pdf	#f
Molecular Weight	kg/kgmol	constant	31.9988
Standard State Enthalpy	j/kgmol	constant	-847.64045
Standard State Entropy	j/kgmol-k	constant	205041.62
Reference Temperature	k	constant	298.15

Material: (ch4 . pdf-mixture) (fluid)

Property	Units	Method	Value(s)
Density	kg/m3	pdf	#f
Molecular Weight	kg/kgmol	constant	16.04276
Standard State Enthalpy	j/kgmol	constant	-74892973

Standard State Entropy j/kgmol-k constant 186057.77

Reference Temperature k constant 298.15

Speed of Sound m/s none #f

Cell Zone Conditions

Zones

name id type

---

stepupworkingfluids 3 fluid

Setup Conditions

Boundary Conditions

Zones

name id type

---

oxidizer_inlet 13 mass-flow-inlet

fuel_inlet_4 23 mass-flow-inlet

fuel_inlet_3 22 mass-flow-inlet

fuel_inlet_2 21 mass-flow-inlet

fuel_inlet_1 20 mass-flow-inlet

wall-stepupworkingfluids 1 wall

outlet 14 pressure-outlet

wall_cooling 33 wall

Setup Conditions

oxidizer_inlet

Condition Value

Mass Flow Rate (g/s)	65.000003
Total Temperature (k)	300
Supersonic/Initial Gauge Pressure (psi)	94.999998
Direction Specification Method	1
Coordinate System	0
X-Component of Flow Direction	1
Turbulent Dissipation Rate (m2/s3)	1
Turbulent Intensity (%)	5
Turbulent Length Scale (mm)	1000
Hydraulic Diameter (mm)	21.800001
Turbulent Viscosity Ratio	10
External Black Body Temperature Method	0
Black Body Temperature (k)	300

fuel_inlet_4

Condition	Value
Reference Frame	0
Mass Flow Specification Method	0
Mass Flow Rate (g/s)	4.5000002
Total Temperature (k)	300
Supersonic/Initial Gauge Pressure (psi)	94.999998
Direction Specification Method	1
Coordinate System	0
X-Component of Flow Direction	1
Turbulent Intensity (%)	5
Turbulent Length Scale (mm)	1000

Hydraulic Diameter (mm) 2.8000001

Turbulent Viscosity Ratio 10

Black Body Temperature (k) 300

outlet

Condition	Value
Gauge Pressure (psi)	0
Backflow Total Temperature (k)	300
Backflow Direction Specification Method	1
Coordinate System	0
X-Component of Flow Direction	1
Backflow Hydraulic Diameter (mm)	1000
Backflow Turbulent Viscosity Ratio	10
External Black Body Temperature Method	0
Black Body Temperature (k)	300
Targeted mass flow (g/s)	1000
Upper Limit of Absolute Pressure Value (psi)	725.18872
Lower Limit of Absolute Pressure Value (psi)	0.00014503774

wall_cooling

Condition	Value
Wall Thickness (mm)	1
Heat Generation Rate (w/m3)	0
Material Name	aluminum
Thermal BC Type	2
Temperature (k)	300
Heat Flux (w/m2)	0

Convective Heat Transfer Coefficient (w/m2-k) 105000

Free Stream Temperature (k) 300

Solver Settings

Equations

Equation	Solved
Flow	yes
Turbulence	yes
Energy	yes
P1	yes
Pdf	yes

Numerics

Numeric	Enabled
Absolute Velocity Formulation	yes

Relaxation

Variable	Relaxation Factor
Density	1
Body Forces	1
Turbulent Kinetic Energy	0.75
Turbulent Dissipation Rate	0.75
Turbulent Viscosity	1
Energy	0.75
Temperature	0.75

P1 1

Mean Mixture Fraction 0.75

Mixture Fraction Variance 0.75

Linear Solver

Variable	Solver Type	Termination Criterion	Residual Reduction Tolerance
Flow	F-Cycle		0.1
Turbulent Kinetic Energy	F-Cycle		0.1
Turbulent Dissipation Rate	F-Cycle		0.1
Energy	F-Cycle		0.1
P1	F-Cycle		0.1
Mean Mixture Fraction	F-Cycle		0.1
Mixture Fraction Variance	F-Cycle		0.1

Pressure-Velocity Coupling

Parameter	Value
Type	Coupled
Pseudo Transient	yes
Explicit momentum under-relaxation	0.5
Explicit pressure under-relaxation	0.5

Discretization Scheme

Variable	Scheme
Pressure	Standard
Density	First Order Upwind
Momentum	Second Order Upwind

Turbulent Kinetic Energy First Order Upwind

Turbulent Dissipation Rate First Order Upwind

Energy First Order Upwind

Mean Mixture Fraction First Order Upwind

Mixture Fraction Variance First Order Upwind

Solution Limits

Quantity Limit

Minimum Absolute Pressure 1

Maximum Absolute Pressure 5e+10

Minimum Temperature 1

Maximum Temperature 5000

Minimum Turb. Kinetic Energy 1e-14

Minimum Turb. Dissipation Rate 1e-20

Maximum Turb. Viscosity Ratio 100000

VITA

Brian Lovich graduated with a Bachelors in mechanical engineering from the University of Texas at El Paso in May of 2015 and went on to obtain his Masters in May 2017. He was a co-author on the AIAA best paper award of 2016 and was on the Deans' list from 2014 onward. He went on an internship with the Department of energy to the National Energy Technology Laboratory in Albany Oregon during the summer of 2016.

Contact Information: bmlovich@miners.utep.edu

This thesis/dissertation was typed by Brian Lovich